PAPER NAME

Radio.pdf

AUTHOR

Devika

WORD COUNT

14765 Words

CHARACTER COUNT

69887 Characters

PAGE COUNT

55 Pages

FILE SIZE

1.5MB

SUBMISSION DATE

Jul 27, 2023 9:59 AM GMT+5:30

REPORT DATE

Jul 27, 2023 10:00 AM GMT+5:30

18% Overall Similarity

The combined total of all matches, including overlapping sources, for each database.

- 15% Internet database
- 13% Publications database
- Crossref database
- Crossref Posted Content database
- 3% Submitted Works database

Excluded from Similarity Report

- Bibliographic material
- Quoted material
- Cited material
- Small Matches (Less then 15 words)
- Manually excluded text blocks

RADIO EVOLUTION OF A CORE - COLLAPSE SUPERNOVA: SN 2008ax

A project report submitted in partial fulfillment for the award of the degree of

Master of Science in **Space Science** (2021-2023)

Submitted by:

Name : Devika V S

Reg No : **210011023197**

Department of Physics

Bharata Mata College

Thrikkakara

Under the guidance of

Dr. Nayana A.J.

DST INSPIRE Faculty

Indian Institute of Astrophysics, Banglore

CERTIFICATE

Certified that the project report entitled **RADIO EVOLUTION OF A CORE - COLLAPSE SUPERNOVA: SN 2008ax** submitted by **DEVIKA V S** for the partial fulfillment for the award of the degree of **Master of Science in Space Science** of Mahatma Gandhi University, Kottayam, Kerala is the bonafide student of Bharata Mata College, Thrikkakara. The project embodies the original results of research work carried out at the Indian Institute of Astrophysics, Banglore under my supervision and guidance. The work presented in this report has not been submitted for the award of any other degree or diploma to any other University or Institution. The project report has been approved as it satisfies the academic requirement respect of project work prescribed by the institution for the said Degree.

JUNE 2023 **DR. Nayana A.J.**

Banglore **DST INSPIRE Faculty**

Indian Institute of Astrophysics

Banglore

ACKNOWLEDGEMENTS

I would like to express my deepest appreciation and gratitude to all those who have contributed to the successful completion of this project. Without their support, guidance, and encouragement, this endeavor would not have been possible.

Firstly, I would like to express my heartfelt gratitude to my supervisor **Dr. Nayana A J**, for her invaluable guidance, expertise, and continuous support throughout this project. Her knowledge and insights have been instrumental in shaping the direction of this research and ensuring its quality.

I am also indebted to my tutor **Dr. Manesh Michael**, who have provided an enriching academic environment and resources for my project. His commitment to excellence in education has been a constant source of inspiration.

I would like to extend my gratitude to all the Faculties of the Department of Physics, Bharata Mata College for their valuable suggestions and support provided during the project period.

My gratitude extends to my friends and family for their unwavering support, encouragement, and understanding throughout this project. Their belief in my abilities and their words of encouragement have been a driving force behind my determination to see this project through to its completion.

I am also grateful to Adv. S S Harikrishnan for his constant support and cheering. His valuable suggestions and contributions helped a lot in the completion of this project.

I would also like to acknowledge the contributions of Mr. Sarath Prabhavu, who have provided valuable feedback and coding ideas, which have greatly enriched my research.

Lastly, I am grateful to all the authors, researchers, and scholars whose works have formed the foundation of this project. Their pioneering efforts and groundbreaking contributions have paved the way for advancements in this field.

Abstract

Core-collapse supernovae (CCSNe) are energetic explosions that happen towards the end stages of the life of a massive star. They show a wide range of observational properties owing to the variety in their progenitor systems. Radio observations and modeling are unique tools to understand the progenitor scenario and environmental properties of CCSNe. In this project, I studied the radio properties of a type IIb core-collapse supernova - SN 2008ax. This study provides a deeper understanding of the evolution of radio flux densities, shock radius, mass loss rate, and other specific characteristics of this supernova which help us to understand the nature of its progenitor. For this, I looked at the radio data of SN 2008ax from $\sim$ 4 to 82 days post-explosion at frequencies 4.86, 8.46, and 22.46 GHz. I modeled the radio light curves using a standard self-absorbed synchrotron emission model (SSA). I derive the shock radii, magnetic fields, and mass-loss rate of the progenitor star multiple epochs from the best-fit modeled parameters. This study of SN2008ax adds to the small sample (only 14 of them)of type IIb supernovae with well-sampled radio observations and modeling results. Thus our study adds to the relatively less explored phase space of radio properties of type IIb supernovae.

This project mainly consists of six chapters where the first and second chapters are the theory which helps better understand the project. In the third chapter, I discussed and enlisted my information on SN 2008ax. The core of my project is chapter four which mainly consists of spectral analysis and modeling results. The following chapter is the discussion chapter which actually discusses the intention of my project and also I have concluded my understanding and inferences in this chapter. My project plans to study the variation of SN 2008ax from other supernovae by studying its radio properties and thereby appending the nature of its progenitor star.

Contents

Chapter 1

Introduction to Supernovae

1.1 SUPERNOVAE

The term Supernova refers to the class of explosive stars located in many galaxies including our own Milky Way galaxy (Alsabti et al. 2017). Supernova is a stage in which the life of stars ends as a result of powerful explosions. When the lifetime of a star came to an end it runs out of fuel or energy stored by nuclear fusion and this condition leads to the collapse of its entire mass towards its core. The mass concentrated in the core become uncontrollable by the gravitational pull, leading to this massive explosion. The energy emitted by a supernova explosion in one second is approximately equal to the energy that the sun emits in a period of 1 million years.

Supernova explosion leaves behind various remnants mostly gaseous remnants and compact stellar remnants. The structures resulting from the explosion of a star in a supernova are the remnants. They are heating the interstellar medium, distributing heavy elements throughout the galaxy, and accelerating cosmic rays. The supernova remnant is leaped by an expanding shock wave and consists of ejected material expanding from the explosion and the interstellar material it drags and shocks along the way. Compact objects, such as white dwarfs, neutron stars, and supermassive black holes, are referred to in the stellar remnants. The smallest and densest star in the universe is neutrons, which reside between normal stars and black holes. They're about 12 miles long, so dense that a teaspoon of material would weigh 1 billion tonnes. They're 10 billion times stronger than steel and have a smooth crust of pure neutrons. In space, a black hole is a place where gravity pulls so much that even light can't escape. Gravity has such strength because it squeezes the material into a small space. It can happen while a star's dying. When the center of a great star falls on its own, or when it disintegrates and creates a supernova, there are stellar black holes. There's a great difference between neutron stars and black holes, Unlike a dark hole, neutron stars would have an even harder surface. A low or medium-mass star, less than 8 times the mass of our sun, would turn into a white dwarf. A white dwarf is about the size of the Sun, but it's a bit smaller in comparison to Earth. This makes white dwarfs one of the densest forms of matter, surpassed only by neutron

stars and black holes. Type Ia supernovae are explosions of white dwarfs which leave no stellar remnants. Several strange high-energy phenomena like X-rays, gamma rays, and radiation from these objects are created by exceptional conditions around those objects. The objects tend to be extraordinarily luminous and have a very strong impact on their surroundings. These remnants have a vital influence on the surrounding interstellar medium. Simultaneous and multiple supernova events lead to a strong impact on the local galactic region and the entire galaxy. A supernova, according to various studies, occurs at a rate of ~ 2 per century per galaxy, leading to a variety of observations with different scientific characteristics. These phenomena may be photometric and spectroscopic, as well as other forms of observation including neutrino physics, cosmic rays, or gravitational waves.

Supernova is the main source of many elements present in the periodic table. These elements are given out to the interstellar medium and are injected into the molecular cloud and serve as the raw material for the formation of stars and other planetary systems. Explosions close to the sun will deposit various isotopes like Fe^{60} on Earth and Moon which have a high influence on the solar system. Cosmic rays produced within the shell of supernova remnants will affect the climatic conditions with everlasting effects.

The study of supernovae is very important since it connects all fields of research in astronomy and it covers all integrative topics than any other objects studied in astronomy. The theoretical study of supernovae along with observational science started in the 1930s and led to the understanding of brightness, light curves, and spectra. The connection between observational data and theoretical possibilities is a relevant topic of discussion even in the present day. The study of the SN explosion has remained front and center because it helps us find out what progenitor stars' properties are. A progenitor star is a star that has erupted into supernovae. For example, the star below the Chandrasekhar limit (greater than 8 $M_{\odot}$) is the progenitor for a white dwarf. Similarly, the massive star which becomes a supernova can be a progenitor for a supernova. The study of a progenitor star that's collapsing to neutron stars or black holes is destroyed to form a diffuse nebula can lead to different inner layers of observations. The nucleosynthesis process creates new elements and at the time of the explosion, these elements are scattered into the interstellar medium. The remnants of supernovae affect the environment of interstellar space since the amount of energy produced will influence the evolution of the galaxy. Our solar system can be viewed through the vision of a supernova since it has a particular role in creating the initial constituents for the solar system's formation. Residuals and residues of an explosion can be spotted in the neighborhood of the sun, moon, and interplanetary dust, affecting the planetary climate and the weather in space. It has also been found that the neutrinos that emerged from the explosion affect the structure of amino acids thus affecting the origin of life on Earth.

1.2 PROGENITOR STARS

1.2.1 White Dwarf

A white dwarf is composed mostly of electron-degenerate matter (Alsabti et al. 2017). It is very thick and has a mass equivalent to that of the sun, while its volume is similar to Earth's. The white dwarfs are the stars that burned all the hydrogen that they once used as nuclear fuel. The fusion in the star's core creates heat and exterior pressure, but it is kept at a balanced level by an internal force of gravity generated by the mass of the star. Gravity forces the star to collapse on itself when hydrogen used as fuel is lost, and fusion slows. Fusion in a star's core produces heat and outward pressure, but this pressure is kept in balance by the inward push of gravity generated by a star's mass. The emission of remaining heat energy produces the White Dwarf's faintest light. There's no fusion going on in a white dwarf. They are stars with hydrostatic equilibrium that depends on the electric degeneracy pressure, and only if a star is under some weight of about 1.4 $M_{\odot}$ can it be achieved. Since this is shown by Subrahmanyan Chandrasekhar, the mass limit is called the Chandrasekhar limit. More than this limit, the white dwarf star will disintegrate and appear to be a supernova. It's because of this gradual accumulation of matter by the nearby star, so that if a white dwarf near the edge of the Chandrasekhar limit has been accreted with mass from its partner, which is referred to as a donor star, then it can be pushed further out into space. It leads to the formation of thermonuclear explosions with an intense flame spreading through the White Dwarf's body. Carbons, oxygen, and silicon are the most important elements of a White Dwarf. The fusion of these nuclei releases energy and increases the star's temperature, which pushes the white dwarf into a supernova explosion. Heavy elements in the iron category such as Co^{56} and Ni^{56}, whose radioactive decay powers the supernova's light curve, are produced by a thermonuclear fusion process.

The progenitor white dwarf star is formed by the evolution of a star whose mass was as much as eight solar masses, which has converted its initial hydrogen into heavier elements or lost itself to space through the stellar wind. That's why the spectrum of supernova doesn't show any hydrogen. Type Ia is the name given to such a supernova spectrum.

1.2.2 Core-Collapse Supernovae

The evolution of massive stars leads to the core of major elements, which in most cases are iron, and for the least massive stars in this range, a mixture of oxygen, neon, magnesium, and silicon. The core is essentially a white dwarf since it is electron degenerate, but it is encircled by a material envelope that may include hydrogen, which will undergo nuclear fusion to produce elements heavier than hydrogen. The progenitor star's initial mass, history of mass loss, metallicity, presence in a binary star system, and the relative proximity and mass of its

companion during evolution all affect the precise shape of the envelope. Core-collapse supernovas (CCSNs) are produced by such stars, which have starting masses that are above 8 solar masses but below 140 solar masses.

A CCSN is referred to as Type II if it exhibits hydrogen spectral lines in its spectrum that are caused by leftover hydrogen in the progenitor's envelope. If helium is present in the composition, the CCSN is referred to as Type I. A CCSN's energy output is influenced by the mass and structure of the progenitor star. Because stars with masses more than 8 $M_{\odot}$ have a range of structures, the luminosity of the CCSN is extremely varied. "Ultra-faint SNe" refers to some extremely faint Type II-P supernovae. While some Type Ic SNe are "broad-lined" or "hyper-novae," others are "super-luminous" SNe. Long-duration gamma-ray bursts may also originate from high-energy supernovae.

Reactions in a Typical Core-Collapse Supernova

In less than a second, the core of a CCSN collapses and becomes a compact stellar object, either a neutron star or a black hole. A neutron star forms when the progenitor's initial mass is less than or equal to 40 solar masses, whereas a black hole forms when it is more massive. The majority of the collapse energy is released as neutrinos during this collapse, which raises the material's temperature to a high level. The envelope material is heated by the neutrinos and is pushed outside to form supernova remnants. Indicating to the outer world that the core has collapsed and the supernova phenomenon is beginning, further neutrinos leave the progenitor. Significant energy is lost in a nonspherical collapse in the form of gravitational waves, which also help to announce the core collapse.

The particles will bounce off the neutron star's hard surface if the collapse results in the production of one, creating a shock wave that will take an hour to reach the progenitor's surface. The material immediately around the shock is heated, raising the temperature by a million degrees. The second indication that a supernova has occurred is the abrupt heating and brightness of the progenitor star's surface and the subsequent ultraviolet photons that are released in a flash and last for a few minutes. The progenitor star's outer layers begin to spread out, enlarging it by a factor of 10 or more in just one day and boosting its brightness by a factor of roughly 1000. The third phase, in which the star begins to display features of a "new star," begins a day or so after the core collapses. The supernova keeps growing indefinitely, its outer layers start to get lighter after a week, and finally, its photosphere starts to compress. It starts to fade after achieving its greatest brightness.

Since there is no hard surface in a black hole, material falling into it cannot bounce. As a result, there is no external shock, and the amount of energy stored in the envelope decreases. As a result, the supernova will lose strength and become fainter than usual. The supernova phenomena will significantly weaken, and the progenitor star's entire mass will be absorbed by the black hole, leaving no trace behind. If a star rapidly collapses into itself without producing

a substantial outflow, this is known as a supernova, and the star vanishes.

The star material is heated to high temperatures and compacted to high densities during the core collapse. Nuclear reactions produce Ni^{56}, which has a half-life of 6 days and decays into Co^{56}, which has a half-life of 77 days and is radioactive. Co^{56} then decays into Fe^{56}, which is stable. The Co^{56} decay produces a variety of gamma rays, one of which has an energy of 847 MeV. A few weeks after the core collapse, the explosion's material expands, becoming lumpier as a result. This permits gamma rays to leave the supernova.

Nucleosynthesis

The production of chemical elements in stars through nuclear fusion events is known as stellar nucleosynthesis. Since the first production of lithium, helium, and hydrogen during the Big Bang, it has happened. The heavier elements are created from hydrogen through nuclear reactions that power the stars. These substances are dispersed into the interstellar medium by supernova explosions. However, nuclear reactions used in explosions themselves create new elements. About half of the atomic nuclei heavier than iron are produced via a series of nuclear processes known as the rapid neutron capture process, or r-process. The most neutron-rich stable isotopes of each heavy metal are often created by the r-process. The locations of this process were found to be supernova explosions.

The yields of the elements produced by CCSN and thermonuclear supernovae differ from one another. As the star is shattered, a Type Ia supernova is created by the thermonuclear runaway process that spreads throughout the white dwarf in a matter of seconds. The universe's primary source of iron is SNe Ia. In evolved big stars with a layered structure of alpha elements, type II/Ib/Ic core-collapse supernovae occur. These supernovae cause the explosive nucleosynthesis of heavy elements close to the core, with the outer layers being evacuated. Through the star, the supernova shock wave spreads and creates alpha products. For example, burning carbon yields O, Ne, Mg, etc., while burning neon yields O, Mg, etc., burning oxygen yields Si, S, Ar, Ca, etc., and burning silicon yields Fe, Si, S, Ca, etc.

1.3 Circumstellar Material and Stellar Companions

In their spectra, certain supernovae have narrow hydrogen emission lines, whereas other, more uncommon supernovae exhibit narrow helium emission lines. A suffix is added to them to denote the narrow lines. Type IIn, Type Ibn, etc., as examples. The existence of circumstellar material surrounding the massive progenitor stars of core-collapse SNe is indicated by these small transient emission lines in supernova spectra. Days after the SN explosions, the lines vanish, demonstrating that the material is spatially restricted and came from the explosion. Most likely, the circumstellar material that is swept up in the supernova's gradual expansion is what causes the hydrogen or helium emission.

Any circumstellar material is ionized by the explosion's ultraviolet light, and when material ejected from the supernova collides with circumstellar material, it becomes ionized. When the supernova's debris reaches the surrounding material, it will be collisionally ionized.

Some supernovae's evolutionary build-up to explosion is influenced by binarity. The double-degenerate scenario for Type Ia supernovae, which assumes the merging of two white dwarf stars either gradually through a mass transfer process or more abruptly through a wholesale merger, depends on it.

A supernova explosion from the other star in its binary system will be prevented by a companion star. The brief spectrum signals caused by the supernova's abrupt release of energy result from the companion star's exterior layers being affected, which causes an X-ray and optical flash lasting minutes to days.

A companion star may occasionally be released from its binary system and ejected, primarily because the supernova progenitor's gravitational pull has been turned off as the supernova material moves past the companion and there is no longer a strong enough gravitational pull to keep the companion in orbit. The companion star maintains its orbital velocity in a straight line and transitions into a high-velocity star that travels through the Galaxy's other stars at a speed of about 100 km/s. Runaway stars are those stars.

X-ray binaries are pairs of stars in which the X-rays are generated as the companion star deposits material on the neutron star or black hole. The properties of such binary stars depend not only on the nature of the compact remnant and the separation of the stars but also on the nature of the companion star, whether it is a high-mass star (HMXB) or low-mass (LMXB). X-ray binaries may evolve further through a second supernova explosion to be a binary neutron star or a neutron star-white dwarf binary.

1.4 Nuetron Stars and Blackholes

As the O/Ne/Mg core or iron core collapses in a CCSN, its temperature passes through an order of 10^9 K. The iron nuclei photo disintegrate into alpha particles as a result of interaction with high-energy gamma rays and then protons and neutrons. At yet higher temperatures, the protons combine with electrons to form neutrons through the process of electron capture. At a density of about 10^{26} g.cm^{-3}, neutron degeneracy pressure halts the contraction, creating a neutron star, of mass around 2 solar masses. In the course of its formation in a core-collapse supernova, the presumed neutron star is more massive than the upper limit for such objects or if depending on metallicity, it accretes material that, has begun to eject in the supernova explosion, stalls, and falls back and the neutron star collapses further to a black hole.

Neutron stars with much higher than usual magnetic fields are called magnetars. A magnetar embedded within a supernova may generate sufficient power that the supernova is super-luminous.

1.5 Different Types of Supernovae

Based on observed spectra and light curves, supernovae are classified into many types. SNe is classified into two categories based on spectroscopic observations; Type I and Type II. Type II SNe (SNe II) shows abundant hydrogen lines in their optical spectra whereas Type I SNe (SNe I) does not show hydrogen lines. SNe I are further sub-classified into Type Ia (SNe Ia) and Type Ib/c (SNe Ib/c). In Type, Ia supernovae optical spectra contain Si II lines whereas Type Ib/c supernova contains He I lines. Among SNe Ib/c, SNe Ib shows helium lines in their spectra and SNe Ic does not show helium lines (or very weak helium lines). SNe Ib/c are identified to be core-collapse explosions of massive stars whose progenitors have lost their hydrogen and/or helium layers before the explosion. Thus, they are collectively called stripped-envelope SNe.

SNe II is understood to be core-collapse explosions of massive stars that retain most of their hydrogen envelope at the time of the explosion. They are further classified into Type IIP (SNe IIP), Type IIL (SNe IIL), Type IIn (SNe IIn), and Type IIb (SNe IIb). SNe IIP/IIL are identified based on the shape of their light curve.

There are two types of light curves: Optical light curve and Radio light curve. The study of the optical light curve is called the direct method whereas the study of the radio light curve is called the indirect method. We cannot get any information about the progenitor using the direct method. So in this project, we are making use of the indirect method which is the study of the radio light curve and the radio properties of the supernovae to understand various physical phenomena and also to get a broad idea about the progenitors.

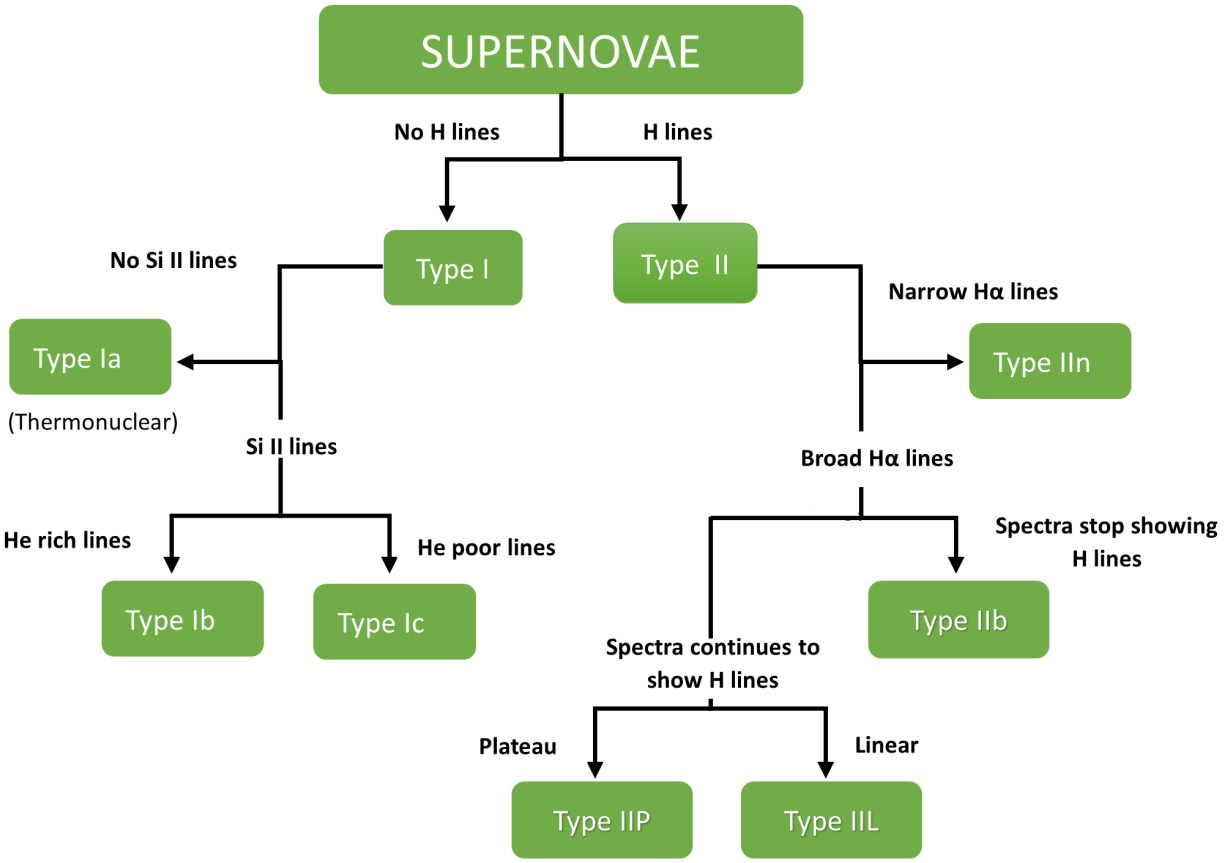

Figure 1.1: Classification of Supernovae based on different properties

Chapter 2

Radio Supernovae

2.1 Radio Emission

The radio emission from SNe arises due to the interaction of the blast wave with the Circumstellar medium. The emission is probably due to electrons from the circumstellar material being accelerated to relativistic energies by the expanding shock waves from the supernova explosion. The explosion of an SN represents the sudden injection of about 10^{51} ergs in an almost point-like region of the space. It causes a large increase in the local pressure, and the disturbed region expands, while the released stellar ejecta begin sweeping up the surrounding gas, driving a shock wave into the interstellar medium (ISM) heating it to very high temperatures. The leading edge of this expanding disturbance is called the shock front. A shock is an irreversible pressure-driven disturbance, a nonlinear plasma wave generated by plasma flow that forms a transition layer that separates supersonic flow (upstream, with Mach numbers that initially can be greater than 1000) to subsonic flow (downstream). Thus the shock marks the location of an invisible wall where density, temperature, magnetic field strength, and flow speed dramatically change. Particles are accelerated at the shock to relativistic energies. Relativistic particles gyrate in the amplified magnetic fields and emit synchrotron radiation (Figure 2.1).

Synchrotron radiation (also known as magneto bremsstrahlung radiation) is the electromagnetic radiation emitted when relativistic charged particles are subject to an acceleration perpendicular to their velocity. The relativistic electrons are thought to be produced by Diffusive Shock Acceleration (DSA). The most efficient process for electrons to gain energy after multiple crossings through a shock wave is called diffusive shock acceleration (DSA), also known as the first-order Fermi acceleration process. It is the acceleration that charged particles undergo when being repeatedly reflected. This is thought to be the primary mechanism by which particles gain non-thermal energies in astrophysical shock waves. Diffusive shock acceleration at the outer front of expanding supernova remnants has provided by far the most popular model for the origin of galactic cosmic rays and has been the

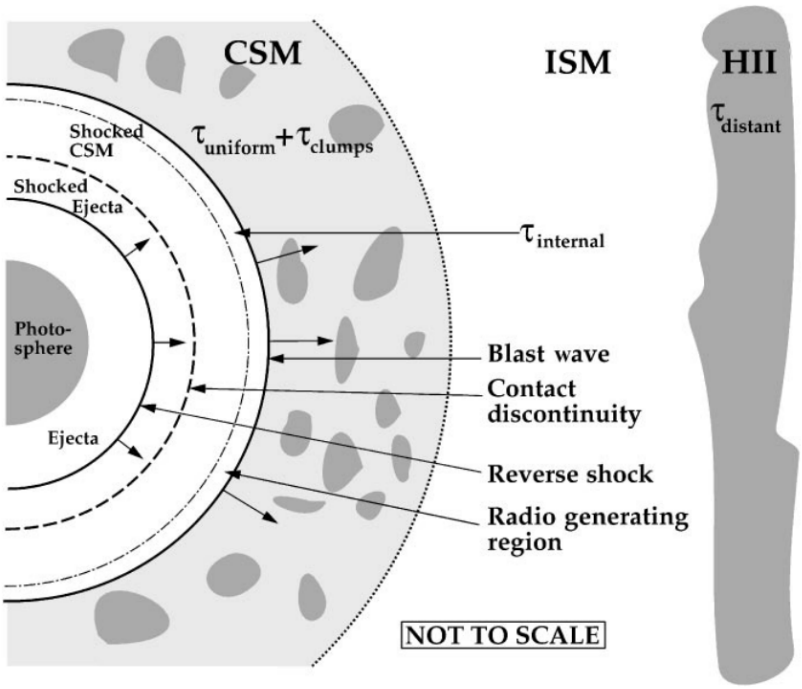

Kurt W Weiler et al. 2002

Figure 2.1: Cartoon, not to scale, of the supernova and its shocks, along with the stellar wind–established circumstellar medium (CSM), the interstellar medium (ISM), and more distant ionized hydrogen (H II) absorbing gas. The radio emission is thought to arise near the blastwave front.

subject of intensive theoretical investigation. DSA explains that the charged particles gain energy by scattering off the magnetic irregularities at the shock every time they cross the shock front. The seed magnetic fields are the circumstellar fields that got compressed and amplified in the interaction region. Even though DSA explains the basic principles of particle acceleration in shocks, it cannot explain the efficiency of particle acceleration for electrons, ions, and the efficiency of magnetic field amplification. Nonthermal electrons produce synchrotron radiation which is detected as radio emission from the Supernova Remnanants. A reverse shock propagates inward, reheating the ejecta. The radio emission detected for core-collapse supernovae thus far has been modeled as synchrotron radiation generated by the interaction of the supernova shock wave with high-density circumstellar material ionized by the initial UV flash. This circumstellar material was most likely thrown off by the progenitor during the late stages of its evolution with models fit to radio observations suggesting that the mass-loss rate may not be constant and the material clumpy. The radio emission of Tycho's SNR has been studied in much detail since its discovery in 1952. It displays a nearly circular thick clumpy shell associated with the ejecta and a thin outer rim along the outer shock that coincides with the X-ray boundary. The radio emission is of synchrotron origin and traces both the population of electrons accelerated to typically GeV energies and the magnetic field.

Type Ib, Type Ic, and Type II supernovae account for radio detections. No Type Ia supernova has been detected in the radio, even though faint radio emission would arise naturally. Type Ia SNe is not radio emitters to the detection limit of the Very Large Array(VLA). VLA is a centimeter-wavelength radio astronomy observatory in the southwestern United States. The VLA comprises twenty-eight radio telescopes (twenty-seven of which are operational while one is always rotating through maintenance) having a length of 25 meters deployed in a Y-shaped array and all the equipment, instrumentation, and computing power to function as an interferometer. Type Ib/c SNe are radio-luminous with steep spectral indices and a fast turn-on/turn-off, usually peaking at 6 cm near or before the optical maximum. They may be fairly homogeneous in some of their radio properties. Type II SNe shows a range of radio luminosities with flatter spectral indices and a relatively slow turn-on/turn-off, usually peaking at 6 cm significantly after the optical maximum. As in the optical, they are quite diverse.

A large number of physical properties of SNe can be determined from radio observations. The properties of the progenitor system and explosion like the mass-loss rate of the progenitor star, density, structure of the CSM, evidence for a binary companion star, etc. can be derived. Very long baseline interferometry (VLBI) imaging shows the symmetry of the blastwave and the local circumstellar medium (CSM), estimates the speed and deceleration of the supernova blastwave propagating outward from the explosion and with assumptions of symmetry and optical line/radio-sphere velocities, allows independent distance estimates to be made. Supernova studies at radio wavelengths provide one of the best means to study the final evolutionary stages of the progenitor before the explosion. The only detected radio emission associated with supernovae has been from pulsars, the spinning condensed remains of the stellar explosions, and from supernova remnants (SNR). The radio emission is supposed to be caused by the slowing down of the GRB(gamma-ray burst) jet as it interacts with circumstellar material, and since it is isotropic, radio observations should pick up off-axis jets. Supernovae which emit radiation at radio wavelengths are known as radio supernovae.

2.1.1 Light Curve

The light curves for radio supernovae have a shape characterized by a rapid rise in flux followed by a slower power-law decline after the maximum is reached at each wavelength. Type Ib and Type Ic supernovae appear to have fairly similar radio properties, arriving at almost the same peak luminosity at 6 cm wavelengths, near or before maximum light at optical wavelengths. The radio light curves of Type II supernovae, however, start much later and are more diverse, peaking at 6cm significantly after the optical maximum. There is some evidence from limited data that radio supernovae may also be useful as distance indicators. In particular, Type Ib and Type Ic supernovae appear to approximate standard candles at radio wavelengths, while the peak luminosity of Type II supernovae at 6cm appears correlated with the time taken to reach that peak from the explosion date. Supernova studies at radio wavelengths provide one of the best means to study the final evolutionary stages of the progenitor before the explosion.

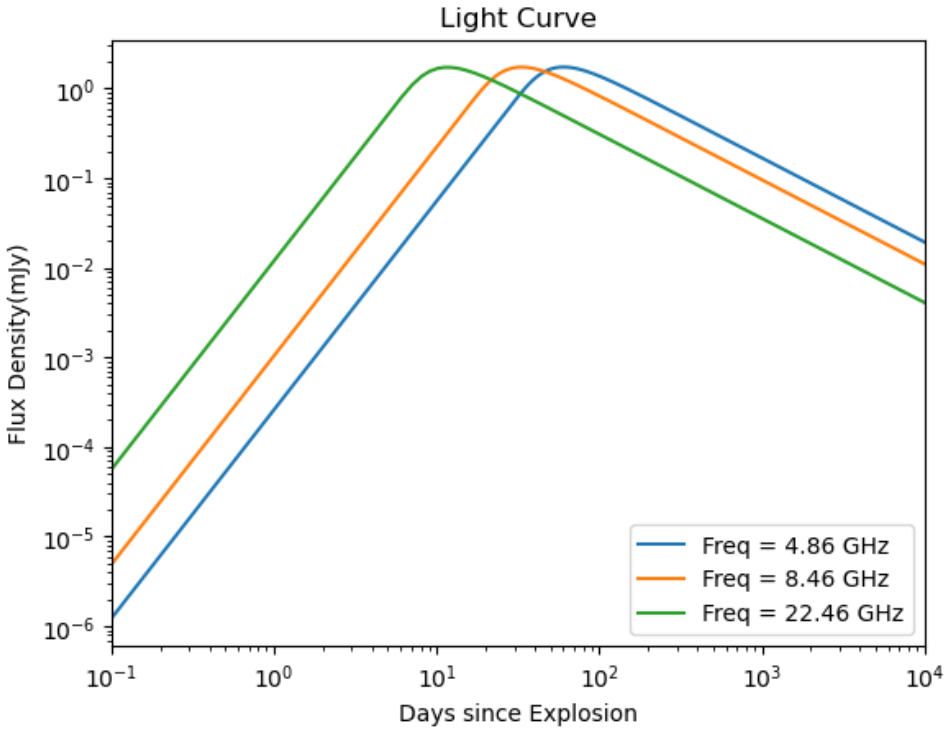

Figure 2.2: Light curve of radio supernova

They also allow astronomers to determine how a radio supernova becomes a radio supernova remnant and may be useful as distance indicators. Measurements of the multifrequency radio light curves and their evolution with time show the density, structure of the CSM, evidence for possible binary companions, clumpiness or filamentation in the presupernova wind, mass-loss rates and changes therein for the presupernova stellar system, and through stellar evolution models, estimates the zero-age main sequence (ZAMS) presupernova stellar mass and the stages through which the star passed on its way to the explosion.

2.1.2 Synchrotron Emission

Synchrotron radiation is generated when relativistic electrons spiral (and hence change velocity) through magnetic fields. Two of its characteristics include power-law energy spectra and polarization. A power law is a functional relationship between two quantities, where a relative change in one quantity results in a proportional relative change in the other quantity, independent of the initial size of those quantities (one quantity varies as a power of another). It is considered to be one of the most powerful tools in the study of extra-solar magnetic fields (magnetic fields generated by the motion of conductive plasma inside a star) wherever relativistic charged particles are present. Most known cosmic radio sources emit synchrotron radiation. It is often used to estimate the strength of large cosmic magnetic fields as well as analyze the contents of the interstellar and intergalactic media. The synchrotron radiation

emitted by an electron of the Lorentz factor in a magnetic field B is around a critical frequency, ν_c which is proportional to the square of the Lorentz factor, γ.

$$\nu_c = \frac{eB}{m_e c}\gamma^2 \tag{2.1}$$

where e and m_e are charge and mass of the electron respectively. B is the magnetic field and c is the velocity of light.

2.1.3 Properties of Radio Emission

- Nonthermal synchrotron emission with high brightness temperature.
- A decrease in absorption with time, resulting in a smooth, rapid turn-on, first at shorter wavelengths and later at longer wavelengths.
- A power-law decline of the flux density with time at each wavelength after maximum flux density (optical depth approximately equals to 1) is reached at that wavelength.
- A final, asymptotic approach of the spectral index to an optically thin, nonthermal, constant negative value.

From the figure, the initial rapid rise in the radio flux density at each frequency is due to the decrease in absorption as the emitting region expands. At all frequencies, there is a smooth transition from an optically thick to a thin regime. The transition happens first at higher frequencies and later to lower frequencies because absorption processes are prominent at lower frequencies. In the optically thin regime, the flux density evolves to a standard nonthermal spectrum with a constant negative spectral index where low frequencies have higher flux density. Due to these two combined effects, the radio flux measurements will be a function of both time and frequency.

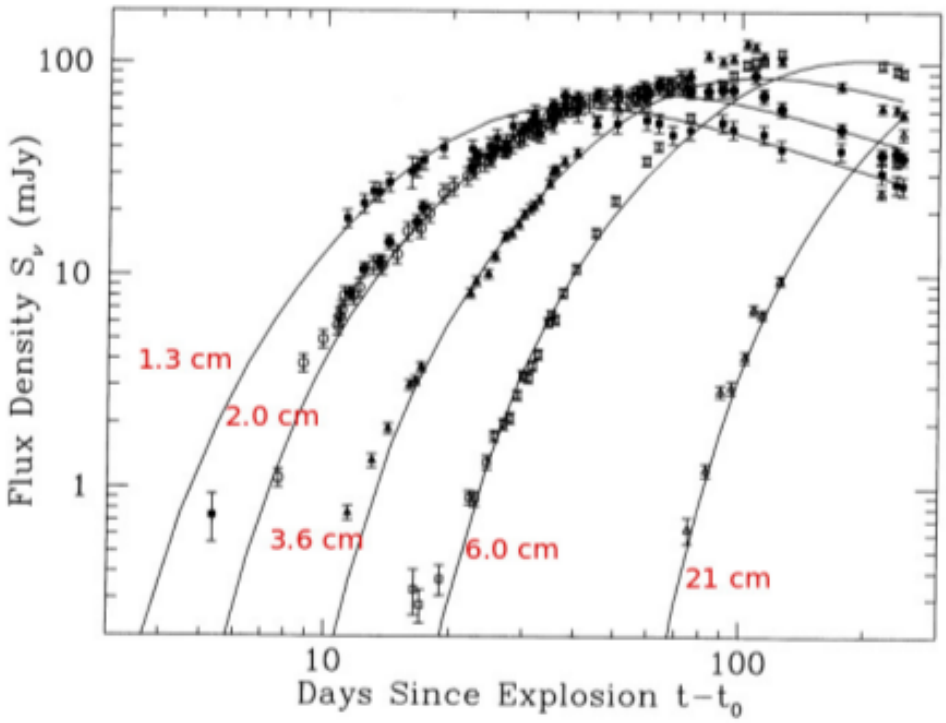

Figure 2.3: The radio light curves of SN 1993J (van Dyk et al., 1994). The numbers in red denote the wavelength. The higher frequency emission turns on first and the lower frequencies turn on later. At each frequency, the light curve makes a smooth transition from an optically thick to a thin regime.

Dyk et al. 1994

2.2 Radio Absorption

The evidence for the presence of relativistic electrons comes from radio observations of SNe. A characteristic is the wavelength-dependent turn-on of the radio emission first seen at short wavelengths and later at longer wavelengths. This behavior is interpreted as a result of decreasing absorption due to the expanding emitting region. Depending on the strength of the post-shock magnetic field and the density of the circumstellar medium, the absorption may be produced either by

- Free-free absorption by material in front of the forward shock front
- Free-free absorption by material within the emitting region
- Synchrotron self-absorption by the same electrons that are responsible for the emission
- The Razin Tsytovich eject

2.2.1 Free free Absorption

FFA arises due to the ionized CSM possibly ionized due to the initial X-ray/UV flash due to the SN explosion. For free-free absorption, the optical depth from the radio-emitting region close to the shock through the circumstellar medium decreases as the shock wave expands, explaining the radio turn-on. For the radio light curves available at that time, free-free absorption by material ahead of the forward shock front provided the best explanation, based on the sharp rise in the supernova flux and the physical conditions expected in and near the emitting region. The optical depth of FFA is defined as

$$\tau_{ffa} = \int_{R_s}^{b} \kappa_{ffa} n_e n_i dr \tag{2.2}$$

where κ_{ffa} is the free-free opacity defined as,

$$\kappa_{ffa} = 3.62 \times 10^{-27} \left(\frac{\nu}{5GHz}\right)^{-2.1} \left(\frac{T}{10^4 K}\right)^{-1.35} \tag{2.3}$$

n_e and n_i are the number densities of electrons and ions in the CSM respectively. The CSM is created by the stellar wind of the progenitor star and hence n_e and n_i are related to the mass-loss rate of the progenitor star. The free-free optical depth scales as $\tau_{ffa} \sim n_e n_i$. As the shock wave

expands through the CSM the density decreases and the FFA optical depth also decreases. The spectral and temporal evolution of FFA radio emission can be analytically represented as

$$S(\nu, t) = K_1 \left(\frac{\nu}{5GHz}\right)^{\alpha} \left(\frac{t}{100days}\right)^{\beta} e^{-\tau_{ffa}} \tag{2.4}$$

$$\tau_{ffa} = K_2 \left(\frac{\nu}{5GHz}\right)^{-2.1} \left(\frac{t}{100days}\right)^{\delta} \tag{2.5}$$

where α is the optically thin spectral index ($F_\nu \propto \nu^\alpha$). Here K_1 and K_2 are the flux density and optical depth normalizations, respectively. t denotes the age of the explosion. The FFA optical depth of the CSM outside the emitting region is proportional to the integral of the square of the CSM density over the radius.

From the radio light curve, or spectrum, the epoch of τ_{ffa} = 1 can be estimated for a given wavelength, and from the line widths in the optical spectrum, the maximum expansion velocity, V can be obtained. The more complete light curves for these supernovae provide strong support for this mechanism, Lundqvist and Fransson (1988) showed how the detailed properties of the circumstellar gas play a role in the absorption process. Both of these are Type II supernovae observed over the years. The optical recovery of these supernovae provides further evidence for a dense circumstellar medium. With the discovery of radio emission from the Type Ib supernova SN 1983N, the turn-on was again attributed to free-free absorption by preshock gas. However, Shklovsky (1985) noted that there was only one point on the rising part of the light curve, so it is not possible to choose the mechanism based on the light curve slope. On the other hand, the brightness temperature of the supernova was high, which suggested the importance of synchrotron self-absorption. Shklovsky further noted that this mechanism did not require a dense wind and suggested that the radio emission might be attributed to a pulsar as opposed to circumstellar interaction.

The FFA optical depth of the CSM outside the emitting region is proportional to the integral of the square of the CSM density over the radius. Assuming a constant stellar wind, $\rho_{CSM} \propto r^{-2}$, thus $\tau_{ffa} \propto R^{-3}$. The blast wave radius evolves as a power law in time, R $\propto t^m$ gives $\tau_{ffa} \sim t^{-3m}$. Thus the temporal index of FFA optical depth (δ) is related to the shock deceleration parameter m as $\delta = -3m$.

Mass-loss rate of progenitor star

The turn-on of the radio emission for RSNe provides a measure of the presupernova mass-loss rate to wind velocity ratio. From the observed absorption process, we can infer various

properties of the stellar wind and the mass-loss rate of the progenitor star. The various assumptions from the calculation are

- The progenitor expels the outer layer of stellar material via a constant stellar wind.
- The wind material is completely ionized possibly due to the initial flash of radiation that has come out of the SN and the wind material has normal chemical abundance.

The radius of the SN ejecta (R) at the time of radio observations is difficult to get unless the SN is very nearby and VLBI observations can be done. The way out is to get the velocities from optical lines during optical maximum and assume that this is the velocity at which SN ejecta is expanding at the time of observation. The shock front radius of SN evolves as R $\propto t^m$, where t denotes the age of the explosion. The FFA optical depth at any given SN ejecta radius R to infinity is given by eqn 2.2, where

$$n_e = \frac{\dot{M}}{4\pi r^2 \omega \mu_e m_H} \tag{2.6}$$

$$n_i = Z n_e \tag{2.7}$$

$$Z = \frac{\sum X_i Z_i^2}{\sum X_i Z_i} \tag{2.8}$$

$$\mu_e = \frac{\sum X_i m_i}{\sum X_i Z_i} \tag{2.9}$$

In the above equations, M is the mass loss rate due to the stellar wind in gs^{-1} where the stellar wind velocity, ν_w is in cms^{-1}. m_H is the mass of a hydrogen atom in grams. X_i, Z_i, and m_i are the number, charge, and mass fraction respectively of the i^{th} ion. Also T in eq (2.3) denotes the electron temperature.

$$\tau_{ffa} = \int_R^\infty \frac{\dot{M}}{4\pi r^2 \omega \mu_e m_H} \bar{Z} n_e \kappa_{ffa} dr \tag{2.10}$$

substituting again for n_e we get

$$\tau_{ffa} = \int_R^\infty \frac{\dot{M}}{4\pi r^2 \omega \mu_e m_H} \bar{Z} \frac{\dot{M}}{4\pi r^2 \nu_\omega \mu_e m_H} \kappa_{ffa} dr \tag{2.11}$$

$$\tau_{ffa} = \int_R^\infty \left(\frac{\dot{M}}{4\pi r^2 \nu_\omega \mu_e m_H} \right)^2 \bar{Z} \kappa_{ffa} dr \tag{2.12}$$

$$\tau_{ffa} = \bar{Z} \kappa_{ffa} \left(\frac{\dot{M}}{4\pi \nu_\omega \mu_e m_H} \right)^2 \int_R^\infty \frac{1}{r^4} dr \tag{2.13}$$

$$\tau_{ffa} = \bar{Z} \kappa_{ffa} \left(\frac{\dot{M}}{4\pi \nu_\omega \mu_e m_H} \right)^2 \left[\frac{r^{-3}}{-3} \right]_R^\infty \tag{2.14}$$

$$\tau_{ffa} = \bar{Z}\kappa_{ffa}\left(\frac{\dot{M}}{4\pi\nu_\omega\mu_e m_H}\right)^2\left[\frac{R^{-3}}{3}\right] \tag{2.15}$$

$$\tau_{ffa} = \frac{\dot{M}^2\bar{Z}\kappa_{ffa}}{3(4\pi)^2R^3m_H^2\mu_e^2\omega^2} \tag{2.16}$$

The radius of the SN ejecta (R) at the time of radio observations is difficult to get unless the SN is very nearby and VLBI observations can be done. The way out is to get the velocities from optical lines during optical maximum and assume that this is velocity at which SN ejecta is expanding at the time of observation.

The shock front radius of SN evolves as R $\propto t^m$.

$$\nu(t) = \frac{dR}{dt} = mt^{m-1} \tag{2.17}$$

$$\nu_i = mt_i^{m-1} \tag{2.18}$$

$$\nu(t) = \nu_i\left(\frac{t}{t_i}\right)^{m-1} \tag{2.19}$$

Thus if we have the velocity at time t_i from optical line observations, we can infer the ejecta velocity at any time 't' using the above equation. Adopting t_i = 45 days for formulation of $\dot{M}$.

$$R = \frac{3.89\times10^{15}}{m}\left(\frac{\nu_i}{10^4 kms^{-1}}\right)\left(\frac{t_i}{45days}\right)\left(\frac{t}{t_i}\right)^m cm \tag{2.20}$$

Substituting R and κ_{ffa} in eq (2.16) and take ν = 5 GHz, we get the expression for $\dot{M}$

$$\dot{M} = 1.47\times10^{20}\tau_{5GHz}^{0.5}\frac{\nu_\omega}{10kms^{-1}}\left(\frac{\nu_i}{10^4kms^{-1}}\right)^{1.5}\left(\frac{t_i}{45days}\right)^{1.5}\left(\frac{t}{t_i}\right)^{1.5m}m^{-1.5}\times\mu_e\bar{Z^{-0.5}}\left(\frac{T_e}{10^4K}\right)^{0.68}gs^{-1} \tag{2.21}$$

Assuming the wind material is singly ionized and has cosmic abundance, we can take $\bar{Z}$ = 1 and μ_e = 1.3. The above equation then becomes

$$\dot{M} = 3.02\times10^{-6}\tau_{5GHz}^{0.5}\left(\frac{\nu_\omega}{10kms^{-1}}\right)\left(\frac{t_i}{45days}\right)^{1.5}\left(\frac{t}{t_i}\right)^{1.5m}\times m^{-1.5}\left(\frac{T_e}{10^4K}\right)^{0.68}M_o yr^{-1} \tag{2.22}$$

The dependence of mass loss rate on t_i is $\dot{M} \propto t_i^{1.5(1-m)}$ and for typical values of m for Type II SNe from observations m = (0.8 to 1), $\dot{M} \propto t_i^{<0.3}$. Thus the dependence of $\dot{M}$ on the time of ejecta velocity measurement is weak.

2.2.2 Synchrotron self absorption

Chevalier 1998 considered the spectrum of a self-absorbed synchrotron emission source with a power-law distribution of relativistic electron energies, E:

$$N(E) = N_o e^{-p} \tag{2.23}$$

where N(E) is the density of relativistic electrons per unit energy, N_o is a constant, and p is the electron spectral index. In the circumstellar interaction model for radio supernovae, the emission is expected to be from a shell, but the details of the emitting region are not known. The shell may be irregular, and the back side of it may be concealed by the supernova.

The observed synchrotron self-absorbed radio emission is given by

$$F_\nu = \frac{piR_s^2}{D^2} S(\nu)[1 - exp(-\tau_{ssa}(\nu))] \tag{2.24}$$

where $S(\nu)$ is the source function and $\tau_{ssa}(\nu)$ is the optical depth of SSA is given by

$$\tau_{ssa}(\nu) = \int_0^s \kappa_{ssa}(\nu) ds \tag{2.25}$$

Here s is the thickness of the emitting slab. For a spherical source, s can be the ratio of emitting volume ($\frac{4\pi R_s^3 f}{3}$) and projected area (πR_s^2), f is the volume filling factor of the emitting region and κ denotes the SSA opacity defined as

$$\kappa_{ssa}(\nu) = c_{abs}(p) N_o B^{(p+2)/2} \left(\frac{\nu}{\nu_o}\right)^{-(p+4)/2} \tag{2.26}$$

$$c_{abs}(p) = 1.183 \times 10^{-41} (p + (10/3)) \Gamma\left(\frac{3p+2}{12}\right) \Gamma\left(\frac{3p+10}{12}\right) \times \Gamma\left(\frac{p+6}{4}\right) \Gamma\left(\frac{p+8}{4}\right)^{-1} \tag{2.27}$$

The source function $S(\nu)$ is

$$S(\nu) = \frac{j(\nu)}{\kappa(\nu)} \tag{2.28}$$

$j(\nu)$ is the synchrotron emissivity

$$j(\nu) = c_{em}(p) B^{(p+1)/2} N_o \left(\frac{\nu}{\nu_o}\right)^{-(p-1)/2} \tag{2.29}$$

where ν_o = 1.253×10^{19} Hz and c_{em} is

$$c_{em}(p) = 4.133 \times 10^{-24} \left(\frac{p + 7/3}{p+1}\right) \Gamma\left(\frac{3p-1}{12}\right) \times \Gamma\left(\frac{p+5}{4}\right) \Gamma\left(\frac{p+7}{4}\right)^{-1} \tag{2.30}$$

Substituting for $j(\nu)$ and $\kappa(\nu)$ in source function, we get

$$S(\nu) = \frac{c_{em}(p)}{c_{abs}(p)} B^{-1/2} \frac{\nu^{5/2}}{\nu_o} \tag{2.31}$$

The value of c_{em} and c_{abs} for p = 3 in c.g.s units are 0.5013×10^{-23} and 4.9697×10^{-41} respectively. The observed synchrotron emission in the optically thick regime will be

$$F_\nu \sim \frac{\pi R_s^2}{D^2} \frac{c_{em}}{c_{abs}} \left(\frac{\nu}{\nu_o}\right)^{5/2} B^{-1/2} \tag{2.32}$$

Thus this part of the spectrum constraints the quantity $R_s^2 B^{-1/2}$. The optically thin part of the spectrum behaves as

$$F_\nu \propto j(\nu) \propto R_s^2 B^{(p+1)/2} N_o \nu^{-(p-1)/2} \tag{2.33}$$

Thus a well-sampled SSA-dominated spectrum and independent constraint on the shock radius R_s will allow us to estimate the electron column density, N_o, and magnetic field strength, B. The blast wave radius can be estimated directly from Very long baseline interferometry (VLBI) observations for bright radio SNe. For eg: the shock radius of SN 1993J was determined from VLBI imaging. The spectral and temporal variation of SSA radio emission from SNe can be analytically represented as (Chevalier 1998)

$$S(\nu, t) = K_1 \left(\frac{\nu}{5GHz}\right)^{5/2} \left(\frac{t}{100days}\right)^{a} (1 - e^{-\tau_{ssa}}) \tag{2.34}$$

$$\tau_{ssa} = K_2 \left(\frac{\nu}{5GHz}\right)^{-(p+4)/2} \left(\frac{t}{100days}\right)^{-(a+b)} \tag{2.35}$$

Here a and b denote the temporal indices of flux densities in the optically thick (F $\propto t^a$) and thin phase (F $\propto t^{-b}$), respectively; τ_{SSA} is the optical depth due to SSA and p is the electron energy power-law index (N(E) $\propto E^{-p}$)

The peak value of the shock radius and the magnetic field is given by

$$R_p = 8.85 \times 10^{15} \alpha^{-1/19} \left(\frac{f}{0.5}\right)^{-1/19} \left(\frac{F_p}{Jy}\right)^{9/19} \left(\frac{D}{Mpc}\right)^{18/19} \left(\frac{\nu}{5GHz}\right)^{-1} \tag{2.36}$$

$$B_p = 0.58 \times \alpha^{-4/19} \left(\frac{f}{0.5}\right)^{-4/19} \left(\frac{F_p}{Jy}\right)^{-2/19} \left(\frac{D}{Mpc}\right)^{-4/19} \left(\frac{\nu}{5GHz}\right) \tag{2.37}$$

The synchrotron intensity at frequency l is given by

$$I_\nu = S(\nu_1) J\left(\frac{\nu}{\nu_1}, \gamma\right) \tag{2.38}$$

The radio light curve of the source is determined by the time dependence of p and N_o.

Mass-loss rate

If SSA is the dominant absorption process, an estimate of the mass-loss rate can be obtained from the magnetic field energy density.

$$U_B = \frac{B^2}{8\pi} = \epsilon_B \rho_{CSM} V_s^2 \tag{2.39}$$

$$\frac{B^2}{8\pi} = \frac{\epsilon_B}{4\pi} \frac{\dot{M}}{\nu_\omega} R_s^{-2} V_s^2 \tag{2.40}$$

$$\dot{M} = \frac{B^2 R_s^2 \nu_\omega}{2\epsilon_B V_s^2} \tag{2.41}$$

Chapter 3

SN 2008ax

3.1 Introduction

SN 2008ax was a helium-rich type IIb core-collapse supernova in the interacting galaxy NGC 4490. SN 2008ax is the second He-rich CC SN that has excellent spectro-photometric monitoring, and for which we can derive direct information on the progenitor, through the analysis of deep pre-explosion archive images. It was discovered independently by Mostardi et al. 2008, on March 3.45 UT) and Nakano & Itagaki (2008, on March 4.62 UT). The new object was around 16th magnitude at discovery. According to Pastorello et al. 2008 the coordinates were $\alpha = 12^h30^m40^s.80$ and $\delta = +41°38'14"5$, quite far ($53"1$ East and $25"8$ South) from the center of the host galaxy. The location had been watched for six hours prior to discovery, and the photos lack any indication of the SN, which limits the time of the explosion breakout to high precision with a small margin of error. At the time of discovery, the new object was about 16th magnitude. It ranked as 2008's third-brightest supernova. About 20 days after the explosion, the brightness in the B-band reached its maximum. X-ray emissions were detected from the event, which is most likely the result of shock heating from the supernova ejecta and circumstellar material. (Pastorello et al. 2008)

Type IIb, Ib and Ic supernovae show a large diversity in observed properties and are referred to as stripped-envelope SNe (SE-SNe). They are distinguished from the majority of all core-collapse events (SNe IIP) by less persistent or absence of hydrogen lines in their early spectra and the lack of a plateau phase in their light curves (Taubenberger et al. 2011). SNe IIb are rather uncommon. Few have been seen thus far, and little is known about how they distribute their mass and energy.

SN 2008ax has been an important study case owing to its small distance and the availability of pre-explosion Hubble Space Telescope (HST) imaging and extensive multi-wavelength follow-up (Folatelli et al. 2015). The progenitor was located using images of the source location of SN 2008ax taken by the Hubble Space Telescope in 2011 and 2013. The photos are consistent

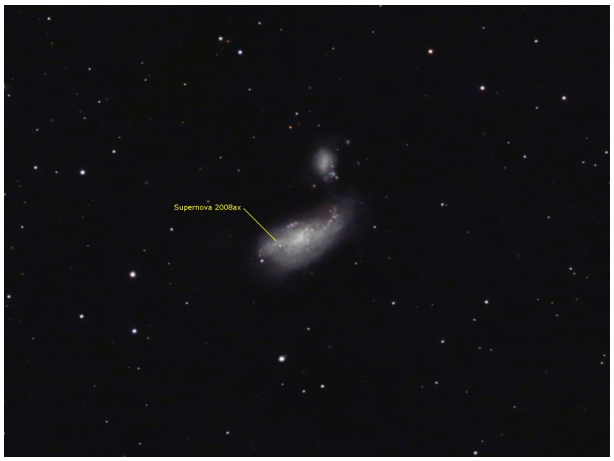

Figure 3.1: SN 2008ax

with a supergiant star of the class B to mid-A type if it were a single star. Models, however, suggest that the progenitor had a relatively modest mass of 4-5 $M_{\odot}$ and an extended hydrogen-rich atmosphere with a radius of 30–40 $M_{\odot}$, which are not in support of this. The progenitor may have been a member of an interacting binary system where much of the atmosphere was lost through mass transfer to the companion, according to a different, more likely model.

3.2 Host Galaxies

A well-known pair of late-type, interacting galaxies, NGC 4490 and NGC 4485, are encased in an extended, asymmetric HI envelope that is elongated perpendicular to the plane of NGC 4490. Clemens(1998) claims that the configuration of the neutral hydrogen envelope might result from a bipolar outflow of H I driven by starburst activity / SN explosions, and not from the interaction between the two companion galaxies. This is in agreement with the particularly high star formation rate estimated in NGC 4490 (Pastorello et al. 2008).

The distance modulus (μ) for NGC 4490 is not well constrained in Pastorello et al. 2008. From Tully (1988) and assuming a Hubble constant H_0 = 72 km/s/Mpc, Pastorello et al. 2008 obtained μ = 29.55 magnitudes. However, Roberts(2002) noted that Tully (1988) gave significantly inconsistent distance estimates for the two interacting galaxies, 9.7 Mpc for NGC 4485 and 8.1 Mpc for NGC 4490.

The P-Cygni H lines are clearly seen in the early-time spectra. About two months after the explosion, these lines start to fade and eventually vanish. He I line became the most prominent spectral feature in the same period. The typical spectrum evolution of a Type IIb supernova is visible in SN 2008ax. The shock breakout of SN 2008ax was delayed by a strict pre-discovery constraint to a window of just a few hours. Its light curve, which peaks in the B band about 20 days after the explosion, strongly resembles that of other He-rich core-collapse supernovae((U, B, V) corresponds to blue (R, I) corresponds to red and (J, H, K) corresponds to near-infrared

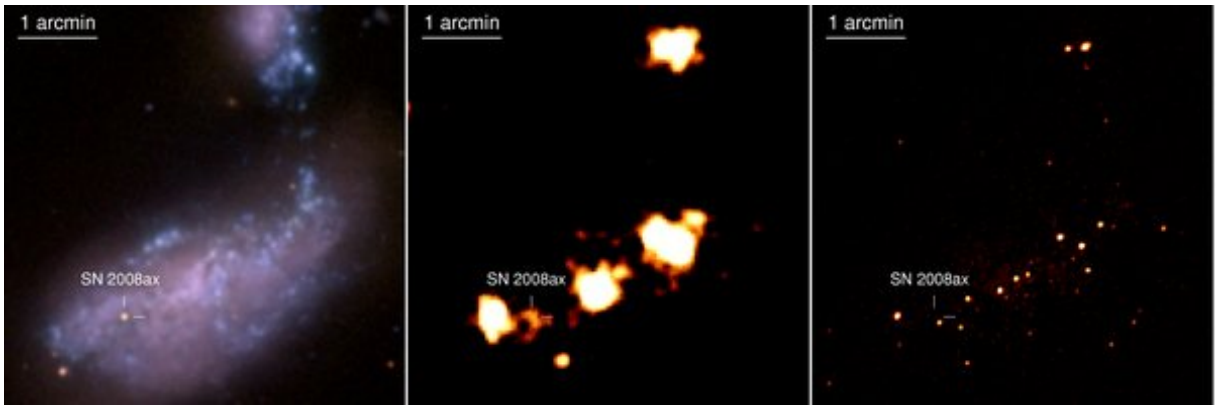

Figure 3.2: Swift UVOT (left), Swift XRT (middle), and Chandra (right) images of SN 2008ax and its host galaxy9 (Roming et al. 2009).

colors). The measured development of SN 2008ax is consistent with the explosion of a young Wolf-Rayet star (of the WNL type), which still had a thin, low-mass shell remaining from its original H envelope. SN 2008ax shares many of the same traits as SN 1993J, with the possible exception of a possibly smaller H mass. This could explain the observations that SN 2008ax's progenitor was a WNL star rather than a K supergiant as was the case with SN 1993J, that SN 2008ax's light curve lacks a notable early-time peak, and that Hα is observed at faster velocities in SN 2008ax than in SN 1993J.

3.3 Distance, Reddening, and Metallicity

in Crockett et al. 2008 the distance to NGC 4490 is estimated]. Pastorello et al. 2008 derived the mean distance modulus of $\mu = 29.92 \pm 0.29$.

Reddening of supernovae refers to the phenomenon where the observed light from a supernova is attenuated and shifted toward longer wavelengths due to the presence of interstellar dust along the line of sight. This reddening effect is caused by dust particles' scattering and absorption of shorter-wavelength (blue) light, while longer-wavelength (red) light is less affected. The amount of reddening depends on the amount of dust along the line of sight to the supernova. This is quantified by a parameter called the color excess (E(B-V)), which measures the difference in color between the observed supernova and its intrinsic color. The color excess is typically determined by comparing the observed supernova spectrum to a template or model spectrum that represents the intrinsic color of the supernova. The reddening of SN 2008ax is estimated as E(B-V) = 0.3 using the equivalent width (EW) of the Na I doublet.

A recent study has estimated the oxygen abundances of NGC 4490 from Sloan Digital Sky Survey Data Release 5 spectra of five individual H II regions (Crockett et al. 2008).Some authors have shown that the H II region abundances in the location of SN 2008ax are comparable to those seen in the central region of M101, where the best current estimates point to solar-like

values. Therefore, it may be said that the SN 2008ax progenitor most likely possessed solar-type metallicity.

3.4 Metamorphosis of SN2008ax

In just a few weeks, SN 2008ax underwent an incredible spectrum evolution, changing through a variety of spectral characteristics. It was initially categorized by Blondin in 2008 as a young type II SN that resembled 1987A. Strong interstellar Na I D absorption that was evident in the spectrum of Londin also indicated that the host galaxy had significantly reddened, E(B-V) = 0.6. Another feature that SN 1987A and significant H and He I lines with blueshifted peaks had in common was extremely quick spectral evolution. The biggest difference was the spectral lines of SN 2008ax, which were substantially wider and corresponded to ejecta velocities between 23000 and 26000 kms^{-1}. They were two-thirds lower in SN 1987A.

Later spectra, however, revealed progressively stronger Fe II, Ca II, and—most importantly—He I characteristics, which indicated that this SN should be reclassified as a type IIb. Chornock further revised the estimate of the host galaxy contribution to the reddening to E(B-V) = 0.5 magnitudes based on a new measurement of the EW of the Na I interstellar doublet (∼0.18nm)

On March 29, 2008, a few days after its maximum, SN 2008ax was also detected in the near-infrared (NIR) using the Triple Spectrograph placed at the 200-inch Hale Telescope. About three to four weeks after the explosion, this spectrum is contrasted with those of the type Ib SN 1999ex and the type II-plateau SN 1999em. The most significant H and He I lines in the NIR area are indicated by dashed blue and red lines for the He I lines, respectively. The P-Cygni line with a peak at 10900 Å is the most noticeable element in all of the spectra. He I 10830Å makes up the majority of SN 2008ax. About 20580 Å is where other He I lines found in the SN 2008ax spectrum can be found. About 20580 Å is where other He I lines found in the SN 2008ax spectrum can be found. Some H is still discernible in the NIR spectrum of SN 2008ax, which is consistent with what we see in the optical spectra. Paschen β, which was conspicuous in SN 1999em, is, in fact, observable (albeit weak) in SN 2008ax at $\lambda \sim 12820$ Å, although it was not unquestionably discovered in the SN 1999ex, a class Ib object.

Other He I lines identified in the spectra of SN 2008ax are at about 20580 Å. In agreement with what we find in the optical spectra, some H is also still visible in the NIR spectrum of SN 2008ax. Paschen β, which was prominent in SN 1999em, is indeed visible (though weak) in SN 2008ax at $\lambda \sim 12820$ Å, while it was not definitely detected in the type Ib SN 1999ex. This is consistent with the classification of SN 2008ax as a type IIb event (Pastorello et al. 2008).

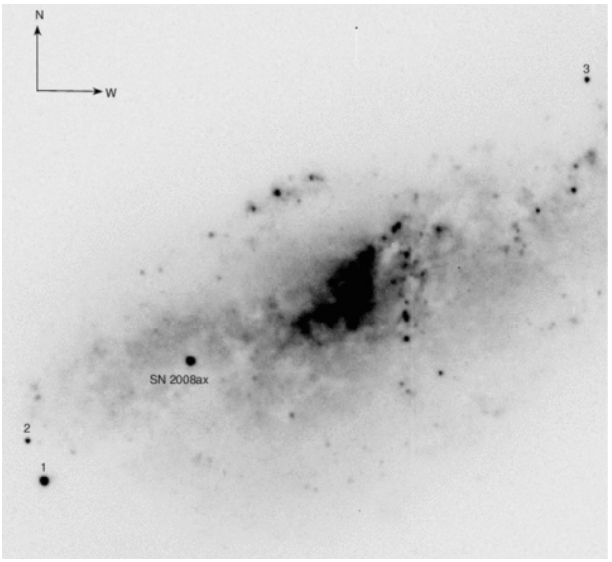

Figure 3.3: SN 2008ax in NGC 4490. V band image obtained on March 22, 2008, with the Liverpool Telescope.(Roming et al. 2009)

Chapter 4

Modelling the Radio Emission from SN2008ax

In this chapter, I'm going to interpret the data of SN 2008ax and discuss the properties of the light curve. The light curve is modeled or curve fitted using the scipy module by finding the best-fit parameters.

4.1 Light Curve

SN 2008ax is one of the best-monitored core-collapse SNe, starting with a deep pre-explosion image obtained only 6 hours before the SN discovery by Mostardi et al. 2008. Soon after its detection, SN 2008ax had an observing campaign that lasted roughly 70 days. Both the 60-inch Palomar Observatory telescope and the 2-m Liverpool Telescope at La Palma, Spain, have collected photometry. The light curve of a supernova is a graph that shows the changing brightness of the supernova over time. It is an important tool for studying supernovae, as it can provide information about the explosion itself and the properties of the star that produced it.

Table 4.1: Supernova Flux Densities or Limits from Radio Observations assuming the date of explosion as 2008 March 3 (Bietenholz et al. 2021)

Name	Obs. Y (year)	Obs. M (month)	Obs. D (date)	Age (Days)	Tel.	Freq. (GHz)	Flux (mJy)	e˙flux (mJy)	σ (mJy)
SN2008ax	2008	3	7	4	VLA-C	8.46	1.19	0.069	0.138
SN2008ax	2008	3	7	4	VLA-C	22.46	5.802	0.593	0.83
SN2008ax	2008	3	10	7	VLA-C	8.46	3.94	0.231	0.457
SN2008ax	2008	3	10	7	VLA-C	22.46	6.742	0.698	0.97
SN2008ax	2008	3	11	8	VLA-C	8.46	4.278	0.235	0.488
SN2008ax	2008	3	11	8	VLA-C	4.86	2.082	0.154	0.259

SN2008ax	2008	3	12	9	VLA-C	8.46	4.63	0.271	0.536
SN2008ax	2008	3	12	9	VLA-C	4.86	3.016	0.183	0.353
SN2008ax	2008	3	13	10	VLA-C	8.46	4.934	0.273	0.564
SN2008ax	2008	3	13	10	VLA-C	4.86	2.934	0.176	0.342
SN2008ax	2008	3	17	14	VLA-C	8.46	4.807	0.262	0.547
SN2008ax	2008	3	17	14	VLA-C	22.46	2.37	0.32	0.398
SN2008ax	2008	3	17	14	VLA-C	4.86	3.993	0.233	0.462
SN2008ax	2008	3	18	15	VLA-C	8.46	4.04	0.226	0.484
SN2008ax	2008	3	18	15	VLA-C	22.46	1.159	0.186	0.219
SN2008ax	2008	3	18	15	VLA-C	4.86	3.646	0.217	0.424
SN2008ax	2008	3	19	16	VLA-C	22.46	1.643	0.203	0.261
SN2008ax	2008	3	19	16	VLA-C	4.86	4.13	0.248	0.482
SN2008ax	2008	3	21	18	VLA-C	8.46	2.631	0.211	0.337
SN2008ax	2008	3	21	18	VLA-C	4.86	3.449	0.241	0.421
SN2008ax	2008	3	26	23	VLA-C	22.46	1.052	0.152	0.185
SN2008ax	2008	3	26	23	VLA-C	8.46	2.748	0.186	0.332
SN2008ax	2008	3	26	23	VLA-C	4.86	3.448	0.277	0.442
SN2008ax	2008	4	1	29	VLA-C	22.46	0.479	0.12	0.129
SN2008ax	2008	4	1	29	VLA-C	8.46	1.396	0.116	0.182
SN2008ax	2008	4	1	29	VLA-C	4.86	2.492	0.193	0.315
SN2008ax	2008	4	3	31	VLA-C	22.46	0.445	0.096	0.106
SN2008ax	2008	4	3	31	VLA-C	8.46	1.13	0.101	0.152
SN2008ax	2008	4	3	31	VLA-C	4.86	1.96	0.175	0.263
SN2008ax	2008	4	7	35	VLA-C	22.46	< 0.249	0.083	0.087
SN2008ax	2008	4	7	35	VLA-C	8.46	0.875	0.088	0.124
SN2008ax	2008	4	7	35	VLA-C	4.86	1.706	0.173	0.243
SN2008ax	2008	4	12	40	VLA-C	8.46	1.023	0.077	0.128
SN2008ax	2008	4	12	40	VLA-C	4.86	1.978	0.202	0.283
SN2008ax	2008	4	16	44	VLA-C	8.46	1.04	0.083	0.133
SN2008ax	2008	4	16	44	VLA-C	4.86	1.694	0.144	0.222
SN2008ax	2008	4	21	49	VLA-C	8.46	0.927	0.081	0.123
SN2008ax	2008	4	21	49	VLA-C	4.86	1.814	0.174	0.251
SN2008ax	2008	4	27	55	VLA-C	8.46	1.382	0.117	0.181
SN2008ax	2008	4	27	55	VLA-C	4.86	2.68	0.301	0.403
SN2008ax	2008	5	1	59	VLA-C	22.46	0.341	0.094	0.1
SN2008ax	2008	5	1	59	VLA-C	8.46	1.028	0.103	0.146
SN2008ax	2008	5	1	59	VLA-C	4.86	2.771	0.232	0.361
SN2008ax	2008	5	8	66	VLA-C	22.46	< 0.671	0.224	0.234
SN2008ax	2008	5	8	66	VLA-C	8.46	0.812	0.103	0.131
SN2008ax	2008	5	8	66	VLA-C	4.86	1.936	0.25	0.316

SN2008ax	2008	5	16	74	VLA-C	8.46	0.453	0.088	0.099
SN2008ax	2008	5	16	74	VLA-C	4.86	1.17	0.103	0.156
SN2008ax	2008	5	21	79	VLA-C	8.46	0.511	0.077	0.092
SN2008ax	2008	5	21	79	VLA-C	4.86	1.581	0.205	0.259
SN2008ax	2008	5	24	82	VLA-C	8.46	0.493	0.062	0.079
SN2008ax	2008	5	24	82	VLA-C	4.86	0.98	0.121	0.156

Note: The C configuration in Very Large Array(VLA) is the third largest configuration, with the antennas spread out over a wider area. Other configurations are A, B, and D where A is the largest and most extended configuration. VLA-C offers improved angular resolution compared to D.

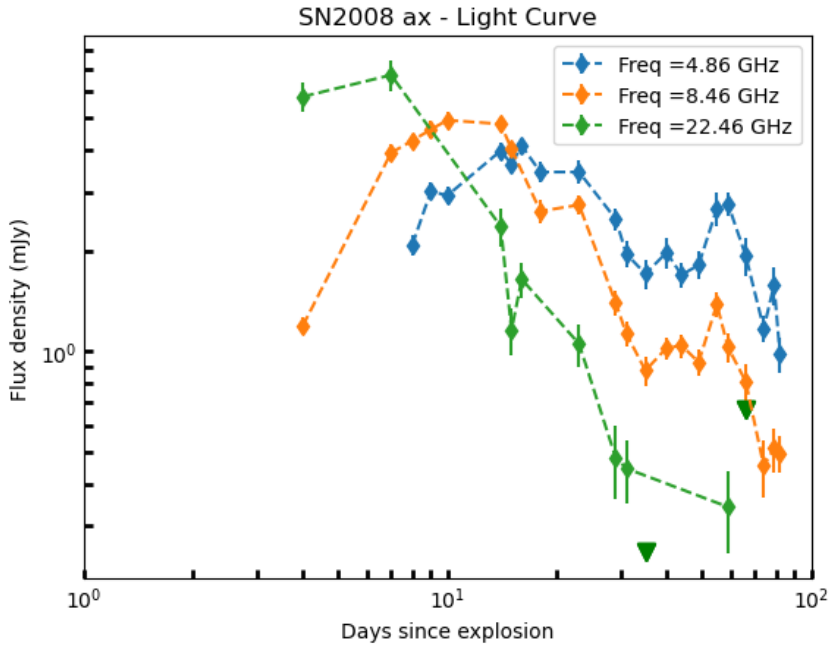

Figure 4.1: The light curve for various frequencies obtained from the details of Table 4.1 where the X axis represents Days since explosion in log scale and the Y axis represents flux density in log scale assuming the date of explosion as 2008 March 3. (Bietenholz et al. 2021)

4.2 Visual Inspection of Radio Light curves

From the light curve, we can infer that it is not a smooth bell shape like other supernova light curves. Also, we can see some irregularities in its structure. Here, the higher frequency (22.46 GHz) is rising first. This is because the synchrotron self-absorption is low for higher frequency. This light curve is characterized by the higher to lower transition or the transition from optically thick to optically thin regime. More irregularities are seen in the optically thin regime. These variations are well described by abrupt density enhancements in the circumstellar medium. The triangular points correspond to the limits. Since the flux density is proportional to the frequency the higher frequency dominates in the light curve. The irregular pattern in the light curve of SN 2008ax is likely the result of a combination of factors, including the structure of the star before the explosion, the amount and distribution of radioactive material, and the interaction of the ejecta with its surroundings. Understanding these factors is important for interpreting supernova observations and improving our understanding of the physics of these explosive events. The interpretation of these irregularities is discussed in the discussion chapter.

One of the important processes in supernovae is the expansion of the supernova ejecta. As the ejecta expands and cools, it emits light at longer wavelengths, causing the supernova to fade over time. The rate of expansion is determined by the amount of energy released in the explosion, as well as the mass and composition of the ejecta. Finally, the interaction of the supernova ejecta with the surrounding interstellar medium can affect the shape of the light curve. As the ejecta

flows through the interstellar medium, it can generate shock waves that heat up and ionize the surrounding gas, producing additional emissions at longer wavelengths.

4.3 Spectral Indices

The spectral index of a source is a measure of the dependence of radiative flux density on frequency. Given the frequency and radiative flux density. Given frequency ν and radiative flux density F_ν, the spectral index α is given by

$$F_\nu \propto \nu^\alpha \tag{4.1}$$

Rearranging the above equation, we get the spectral index as

$$\alpha(\nu) = \frac{\partial log F_\nu(\nu)}{\partial log \nu} \tag{4.2}$$

In this context, we need the equation,

$$\frac{F_1}{F_2} = \left(\frac{\nu_1}{\nu_2}\right)^\alpha \tag{4.3}$$

In the context of data analysis, spectral indices refer to numerical measures that describe the shape or characteristics of a spectrum, which is a plot of the intensity or power of a signal as a function of frequency or wavelength. It can provide valuable information about the properties of a signal or a phenomenon. They can be used to identify specific features or patterns in a spectrum, measure the strength or intensity of certain spectral lines or peaks, quantify the overall shape or slope of a spectrum, and reveal underlying physical or chemical properties of the source of the spectrum. Many different spectral indices can be calculated depending on the specific application and goals of the analysis. Several spectral indices are commonly used in the study of supernovae. They are designed to capture specific features or characteristics of supernova spectra and can provide valuable information about the properties and evolution of these cosmic events.

Table 4.2: Spectral Index calculated for various frequencies using the data from Bietenholz et al. 2021

Sl. No	Obs. Year	Obs. Month	Obs. Date	Age	Spectral Index 8.46/22.46	Spectral Index 4.86/8.46
1	2008	3	7	4	1.62±0.18	- - -
2	2008	3	10	7	0.55±0.02	- - -
3	2008	3	11	8	- - -	1.30±0.07
4	2008	3	12	9	- - -	0.77±0.03

5	2008	3	13	10	- - -	0.94±0.04
6	2008	3	17	14	-0.72±0.04	0.33±0.01
7	2008	3	18	15	-1.28±0.12	0.19±0.01
8	2008	3	19	16	- - -	- - -
9	2008	3	21	18	- - -	-0.49±0.03
10	2008	3	26	23	-0.98±0.10	-0.41±0.02
11	2008	4	1	29	-1.10±0.25	-1.05±0.11
12	2008	4	3	31	-0.95±0.24	-0.99±0.13
13	2008	4	7	35	-1.29±0.55	-1.20±0.19
14	2008	4	12	40	- - -	-1.19±0.16
15	2008	4	16	44	- - -	-0.88±0.12
16	2008	4	21	49	- - -	-1.21±0.18
17	2008	4	27	55	- - -	-1.19±0.12
18	2008	5	1	59	-1.13±0.36	-1.79±0.24
19	2008	5	8	66	-0.20±0.04	-1.57±0.27
20	2008	5	16	74	- - -	-1.71±0.52
21	2008	5	21	79	- - -	-2.04±0.54
22	2008	5	24	82	- - -	-1.24±0.35

The interpretation of the spectral index curve and the reason for its transition from positive values to negative values by increasing age is given in the discussion chapter.

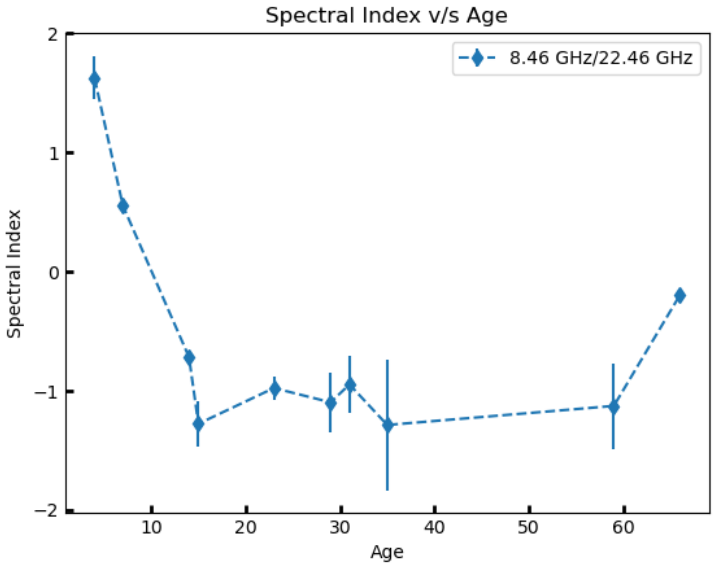

Figure 4.2: Plot of Spectral Index versus age for the frequencies 8.46 GHz and 22.46 GHz using Table 4.2

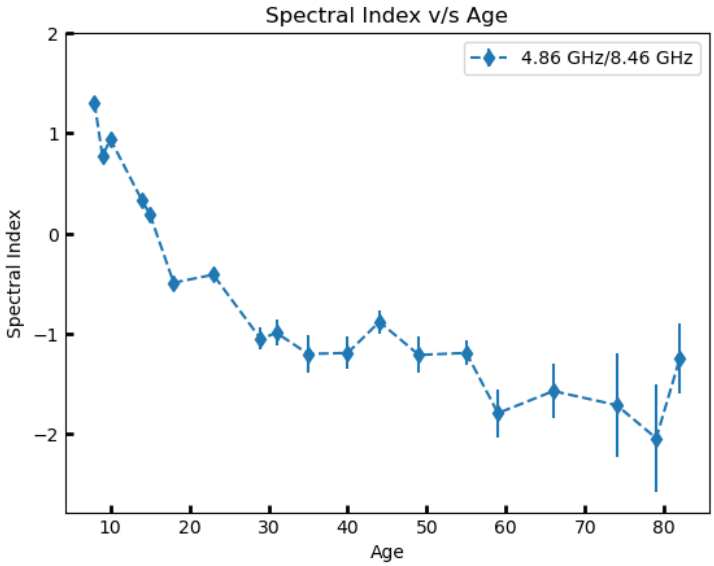

Figure 4.3: Plot of Spectral Index versus age for the frequencies 4.86 GHz and 8.46 GHz using Table 4.2

4.4 Modeling

Modeling of the Light curve of SN2008ax (Figure 4.1) is done using the scipy module. First, we define the function :

$$F(\nu,t) = K_1 \left(\frac{\nu}{5GHz}\right)^{5/2} \left(\frac{t}{100days}\right)^{a} (1 - e^{-\tau_{ssa}}) \tag{4.4}$$

$$\tau_{ssa} = K_2 \left(\frac{\nu}{5GHz}\right)^{-(p+4)/2} \left(\frac{t}{100days}\right)^{-(a+b)} \tag{4.5}$$

where $F(\nu,t)$ is the flux density and τ_{ssa} is the optical depth of SSA.

Here the parameters are K_1, K_2, a, b and p.

Using curve fitting we obtained the best fit values for the parameters as

- K_1 = 3.65112749 $\pm$ 0.5932656931632513
- K_2 = 2.2873868 $\pm$ 0.561850940592897
- a = 2.5879013 $\pm$ 0.2820147838554813
- b = 1.09622549 $\pm$ 0.07365147698236288
- p = 2.76763395 $\pm$ 0.19459833878188687

4.4.1 Reduced chi-squared Value

The reduced chi-squared value is a statistical metric that quantifies the goodness of fit between a model and observed data. It is denoted as χ^2. This value provides a measure of the total discrepancy between the standard model and the data.

and got the value as χ^2 = 3.2069503208648724

- Plotted the light curve for the corresponding three frequencies using the best-fit parameters.

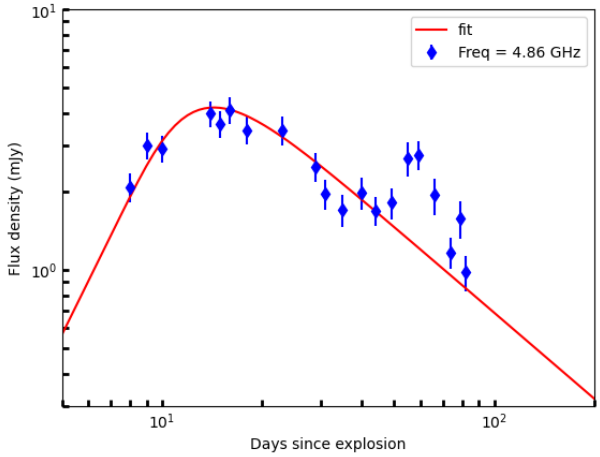

Figure 4.4: Fitted light curve for the frequency 4.86 GHz

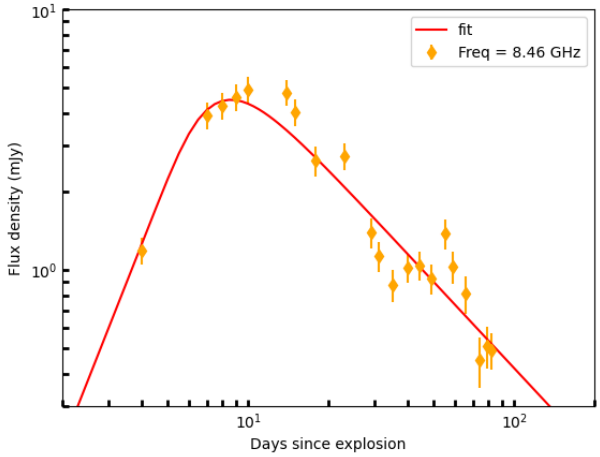

Figure 4.5: Fitted light curve for the frequency 8.46 GHz

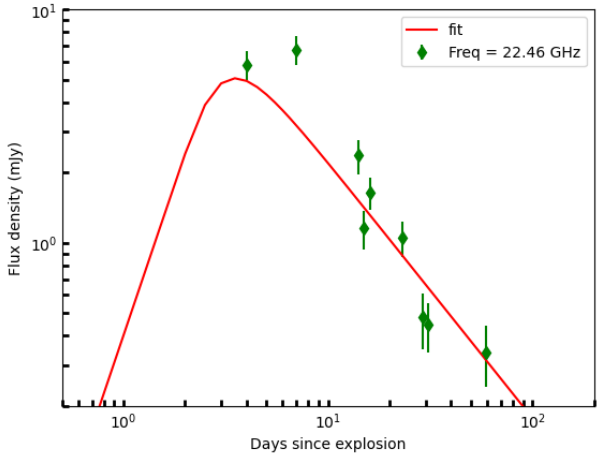

Figure 4.6: Fitted light curve for the frequency 22.6 GHz

```
t = sn_data["Time"]
L = sn_data["Flux"]
nu = sn_data["Freq"]
e = sn_data["Error"]
X = nu,t

def func(X, K1, K2, a, b, p):
    tau_ssa = K2 * (nu/5.0)**(-(p+4)/2) * (t/10)**(-(a+b))
    return K1 * (nu/5)**2.5 * (t/10)**a * (1 - np.exp(-tau_ssa))

K1 = 0.06
K2 = 207.04
a = 2.33
b = 0.94
p = 3.03

popt, pcov = curve_fit(func,X, L, p0 =[K1, K2, a, b, p], sigma = e)

K1_fit = popt[0]
K2_fit = popt[1]
a_fit = popt[2]
b_fit = popt[3]
p_fit = popt[4]

popt, pcov = curve_fit(func, X, L, sigma = e)
popt

perr = np.sqrt(np.diag(pcov))

K1e = perr[0]
K2e = perr[1]
ae = perr[2]
be = perr[3]
pe = perr[4]
print(K1e,K2e,ae,be,pe)

residuals = L - func(X, *popt)

chi_squared = np.sum((residuals**2)/e**2)

n_data = len(L)
n_params = len(popt)
n_degrees_of_freedom = n_data - n_params

reduced_chi_squared = chi_squared / n_degrees_of_freedom
print("Reduced chi-squared:", reduced_chi_squared)
```

```
sn_data_1 = sn_data[sn_data["Freq"]==4.86]
sn_data_2 = sn_data[sn_data["Freq"]==8.46]
sn_data_3 = sn_data[sn_data["Freq"]==22.46]
print(sn_data_1)
print(sn_data_2)
print(sn_data_3)

t1 = sn_data_1["Time"]
L1 = sn_data_1["Flux"]
nu1 = sn_data_1["Freq"]
e1 = sn_data_1["Error"]


def func(t, K1, K2, a, b, p):
    tau_ssa = K2 * (4.86/5.0)**(-(p+4)/2) * (t/10)**(-(a+b))
    return K1 * (4.86/5)**2.5 * (t/10)**a * (1 - np.exp(-tau_ssa))

t = np.linspace(5,500,1000)


fig2,ax = plt.subplots()
ax.errorbar(t1,L1,yerr=e1, label ="Freq = 4.86 GHz" ,fmt = 'db')
ax.plot(t, func(t, *popt), 'r-', label = "fit", linestyle = "-")
ax.set_xlabel("Days since explosion")
ax.set_ylabel("Flux density (mJy)")
ax.set_xscale("log")
ax.set_yscale("log")
ax.set_xlim(5,200)
ax.set_ylim(0.3,10)
plt.tick_params(axis='both', which='both', direction='in', length=4, width=2)
ax.legend()

fitted_flux = func(t, *popt)

peak_flux = np.max(fitted_flux)
peak_time = t[np.argmax(fitted_flux)]
print (peak_flux)
print(peak_time)
```

4.4.2 Peak Values

We found the peak values of flux and time from the fitted light curve and got the values of F_p as:

- For ν = 4.86 GHz, F_p = 4.208 $\pm$ 0.42 MJy
- For ν = 8.46 GHz, F_p = 4.504 $\pm$ 0.45 MJy
- For ν = 22.46 GHz, F_p =5.081 $\pm$ 0.50 MJy

Similarly, we get t_p as

- 14.414 days for ν = 4.86 GHz
- 8.492 days for ν = 8.46 GHz
- 3.5 days for ν = 22.46 GHz

Using F_p and t_p we can calculate the shock radius R_p and magnetic field B_p as (Nayana et al. 2022) :

$$R_p = 8.85 \times 10^{15} \alpha^{-1/19} \left(\frac{f}{0.5}\right)^{-1/19} \left(\frac{F_p}{Jy}\right)^{9/19} \left(\frac{D}{Mpc}\right)^{18/19} \left(\frac{\nu}{5GHz}\right)^{-1} \tag{4.6}$$

$$B_p = 0.58 \alpha^{-4/19} \left(\frac{f}{0.5}\right)^{-4/19} \left(\frac{F_p}{Jy}\right)^{-2/19} \left(\frac{D}{Mpc}\right)^{-4/19} \left(\frac{\nu}{5GHz}\right) \tag{4.7}$$

We have taken the volume filling factor as 0.5 and α as 1. Also, the distance of the supernova in Mpc is 6.2. As an example, taking ν as 4.86 and doing the calculation.

$$R_p = 8.85 \times 10^{15} (1)^{-1/19} \left(\frac{0.5}{0.5}\right)^{-1/19} \left(\frac{4.208 \times 10^{-3}}{Jy}\right)^{9/19} \left(\frac{6.2}{Mpc}\right)^{18/19} \left(\frac{4.86}{5GHz}\right)^{-1} \tag{4.8}$$

$$R_p = (3.82 \pm 0.6) \times 10^{15} cm \tag{4.9}$$

Also,

$$B_p = 0.58 \times (1)^{-4/19} \left(\frac{0.5}{0.5}\right)^{-4/19} \left(\frac{4.208 \times 10^{-3}}{Jy}\right)^{-2/19} \left(\frac{6.2}{Mpc}\right)^{-4/19} \left(\frac{4.86}{5GHz}\right) \tag{4.10}$$

$$B_p = (0.682 \pm 0.07) Gauss \tag{4.11}$$

- For ν = 4.86 GHz, R_p = $(3.82 \pm 0.6) \times 10^{15}$ cm and B_p = (0.682 ± 0.07) Gauss
- For ν = 8.46 GHz, R_p = $(2.27 \pm 0.33) \times 10^{15}$ cm and B_p = (1.18 ± 0.12) Gauss
- For ν = 22.46 GHz, $R_p = (0.908 \pm 0.13) \times 10^{15}$ cm and $B_p = (3.09 \pm 0.32)$ Gauss

4.4.3 Temporal Variation

We have the Power Law equations (Nayana et al. 2022) :

$$\left(\frac{R_1}{R_2}\right) = \left(\frac{t_1}{t_2}\right)^m \tag{4.12}$$

$$\left(\frac{B_1}{B_2}\right) = \left(\frac{t_1}{t_2}\right)^\alpha \tag{4.13}$$

Using these equations we can find the values of m and α.

- For ν = 4.86 GHz, m = 0.983 $\pm$ 0.07 and α = -1.036 $\pm$ 0.04
- For ν = 8.46 GHz, m = 1.033 $\pm$ 0.07 and α = -1.086 $\pm$ 0.04
- For ν = 22.46 GHz, m = 1.015 $\pm$ 0.07 and α = -1.067 $\pm$ 0.04

4.4.4 Mass Loss Rate

$$\dot{M} = \frac{B^2 R^2 \nu_w}{2\epsilon_B V^2} \tag{4.14}$$

Using the values of R_p, R_p and V, we found the values of $\dot{M}$ in $M_\odot yr^{-1}$ for all three frequencies. Taking the value of ν_w = 200 kms^{-1} and ϵ_B = 0.33. Mean Velocity, V can be defined as:

$$V = \frac{R_p}{t_p} \tag{4.15}$$

- For ν = 4.86 GHz,

$$V = \frac{3.82 \times 10^{15} \times 10^{-5}}{14.414 \times 86400} \tag{4.16}$$

$$V = (3.1 \pm 0.5) \times 10^4 kms^{-1} \tag{4.17}$$

Similarly,

- For ν = 8.46 GHz, V = (3.1 $\pm$ 0.4) $\times$ 10^4 kms^{-1}
- For ν = 22.46 GHz, V = (3.0 $\pm$ 0.4) $\times$ 10^4 kms^{-1}

Therefore we can calculate the mass loss rate as:

- For ν = 4.86 GHz,

$$\dot{M} = \frac{0.68^2 \times (3.82 \times 10^{15})^2 \times 200 \times 10^5}{2X0.33 \times (3.06X10^4 \times 10^5)^2 \times 1.989X10^{33} \times 3.17X10^{-8}} \tag{4.18}$$

$$\dot{M} = (3.46 \pm 1.7) \times 10^{-7} M_\odot \, yr^{-1} \tag{4.19}$$

Similarly,

- For ν = 8.46 GHz, $\dot{M}$ = (3.6 $\pm$ 1.6) $\times$ $10^{-7} M_\odot$ yr^{-1}
- For ν = 22.46 GHz, $\dot{M}$ = (3.0 $\pm$ 1.9) $\times$ $10^{-7} M_\odot$ yr^{-1}

```
import numpy as np
from uncertainties import ufloat

F = 4.208
flux_error = 0.42
D = 6.2
D_error = 0.62
nu = 4.86
nu_error = 0.48

F = ufloat(F, flux_error)
D = ufloat(D, D_error)
nu = ufloat(nu, nu_error)

R = 8.8e15 * (F*1e-3)**(9/19) * (D)**(18/19) * (nu / 5)**(-1)
print(R)

B = 0.58*(F*1e-3)**(-2/19) * (D)**(-4/19) * (nu/5)
print(B)

R = 0.908 * 1e15
R_error = 0.13 * 1e15
t = 3.5

R = ufloat(R, R_error)

V = (R*1e-5)/(t*86400)
print(V)

B = 3.09
B_error = 0.32
R = 0.908 * 1e15
R_error = 0.13*1e15
V = 3.0 * 1e4
V_error = 0.4*1e4
nu = 22.46
nu_error = 0.224
nu_w = 200 * 1e5
epsilon_B = 0.33

B = ufloat(B, B_error)
R = ufloat(R, R_error)
nu = ufloat(nu, nu_error)
V = ufloat(V,V_error)

Dot_M = ((B**2 * R**2 * nu_w) / (2 * epsilon_B * (V*1e5)**2))/(1.989*1e33 * 3.17 * 1e-8)
print(Dot M)
```

4.5 Results

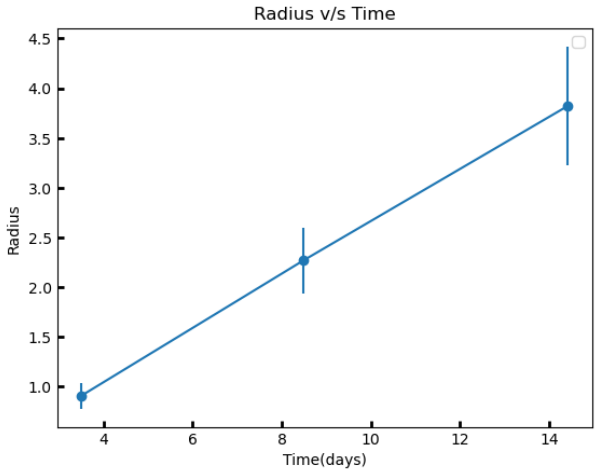

Figure 4.7: The temporal variation of the radius with time.

ν_p (GHz)	F_p (mJy)	t_p (days)	R_p (10^{15}cm)	B_p (Gauss)	V ($10^4 \mathrm{km} s^{-1}$)	$\dot{M}$ ($10^{-7} M_\odot yr^{-1}$)
4.86±0.48	4.208±0.42	14.414	3.82±0.6	0.682±0.07	3.1±0.5	3.4±1.7
8.46±0.84	4.504±0.45	8.492	2.28±0.33	1.18±0.12	3.1±0.4	3.6±1.6
22.46±0.22	5.081±0.50	3.5	0.91±0.13	3.09±0.32	3.0±0.4	4.2±1.9

ν_p	m	α
4.86±0.48	0.983±0.07	-1.036±0.04
8.46±0.84	1.033±0.07	-1.086±0.04
22.46±0.22	1.015± 0.07	-1.067±0.04

Chapter 5

Discussion and summary

In this project, I have carried out a detailed study on the radio emission from a Type IIb supernova SN 2008ax. I modeled the radio light curves of SN 2008ax using the standard model (Chevalier 1998) and obtained various physical parameters.

5.1 Interpretation of Light Curve

Through the star's envelope, the shock wave is caused by the core collapse propagation. It is moving at speeds that are greater than the local speed of sound, which causes a shock wave to occur. When the SW reaches the surface, photon diffusion takes over and energy starts to radiate away. The SW warms and accelerates the matter, depositing mechanical and thermal energy into the envelope's subsequent layers. Soon after the shock emerges, the material's acceleration stops, and the expansion almost completely homogenizes. After the breakout, there occurs a violent expansion that causes the outermost layers to cool and the photospheric radius to expand. After the first shock breakout, adiabatic cooling is thought to be the cause of the light curve's dip.

From the radio light curve of frequencies 4.86 GHz, 8.46 GHz, and 22.46 GHz, we can understand both the basic and usual properties of SN2008ax. We have plotted the light curve (Figure 4.1) using the data from Bietenholz et al. 2021. We can see that the shape of the curve is not a bell shape and I have studied this variation which lead to the understanding of various properties and the associated phenomenon. From the light curve, we can see the first rising curve is the curve of 22.46 GHz which is the highest frequency. This is because the absorption is low for higher frequencies. That is the optical depth depends on wavelength. SN 2008ax shows an irregular pattern in the light curve compared to other Type IIb supernovae. These variations are well described by abrupt density enhancements in the circumstellar medium. One factor that can affect the shape of a supernova's light curve is the structure of the star before the explosion. In the case of SN 2008ax, the star's outer envelope was likely stripped

away before the explosion, leaving a relatively compact core. This could have resulted in a more irregular light curve compared to other type II-P supernovae that have a more extended outer envelope. In addition, the interaction of the supernova ejecta with its surrounding environment can also affect the shape of the light curve. This interaction can produce shocks that heat the surrounding material, which can result in additional emissions at late times. This additional emission can cause irregularities in the light curve.

The region of the first rise of the curve is called the optically thick regime which is attributed to synchrotron self-absorption and the region beyond the peak is called the optically thin regime.

5.2 Spectral Analysis

I have carried out the spectral analysis by calculating the spectral index for frequencies 8.46 GHz and 22.46 GHz and then for frequencies 4.86 GHz and 8.46 GHz. With the increase in the age of supernovae, the spectral index is owing negative values, implying that the intensity increases as the frequency increases. The positive value of the spectral index is due to the synchrotron self-absorption process. We can also see that the spectral index has its higher value at the lower value of age. The flux density is higher for high frequency which is the reason for the negative values.

The temporal evolution of shock wave radius is best fitted by a power law $R \propto t^{0.98\pm0.07}$. We know that the value of m will be 1 for a non-decelerating blast wave. Since the derived value is m $\sim$ 1, this indicates that the blast wave is a non-decelerating one. The temporal index of the postshock magnetic field is best fitted by the equation $B \propto t^{\alpha_B}$ and we get α_B = -1.03$\pm$0.04. α_B can be connected to the CSM density as $\alpha_B = \frac{m(2-s)}{2}$ - 1 which gives s = 2.073.

5.3 Modelling

Since the reduced chi-squared value(χ^2) is 3.206, we can infer that it is not the best fit. Even though there is a deviation from the standard model it is a better representation of observed data. The standard model underestimates the flux densities at multiple frequencies (Figure 4.4). The majority of flux densities in the optically thin region are significantly above the modeled curve. That example, the frequency 4.86 GHz experiences a second bump around t$\sim$ 60 days. This second bump is caused by a rapid increase in flux densities, which may be the result of the forward shock interacting with the CSM's density enhancement. The non-uniform mass-loss rate of a single star progenitor due to stellar winds and the mass stripping by a binary companion are the causes of the density variations. The observational evidence from large stars and supernova remnants strongly suggests that complicated mass-loss processes occur near the end of stellar evolution. The binary parameters will have an impact on the strength of CSM density enhancement and location in a binary star system.

Multiple occurrences of mass-loss events have been attributed to periodic light-curve bumps of modest flux density fluctuations in SN 2003bg (Soderberg et al. 2006) and SN 2001ig (Ryder et al. 2004). They showed variations in the light curve during a period of t = 120-300 days. In SN 2016gkg (Nayana et al. 2022), flux density enhancement is at t$\sim$ 299 days whereas in SN 2008ax we see this enhancement at t$\sim$ 60 days which corresponds to a stellar evolution phase.

5.4 Comparison of SN2008ax with other Type IIb Supernovae

According to Soderberg et al. 2006, the comparison of the radio light curves demonstrates that each supernova's variations are generally distinct from one another. In accordance with their placement in the $F_p - t_p$ diagram, two populations of SNe IIb were identified based on their radio characteristics by Nayana et al. 2022 (Figure 5.2): When SNe IIb has compact progenitors, it is referred to as SNe cIIb, and when it has extended progenitors, it is referred to as SNe eIIb. In comparison to SN 1993J and SN 2001gd, SNe eIIb, the SNe cIIb group, which includes SN 2008ax, SN 2003bg, and SN 2001ig, has faster shocks, a less dense CSM, and a compact progenitor. Due to their thicker CSM from slow stellar winds of extended progenitors, SNe eIIb has slower shocks. The mass loss rate of SN 2008ax is low compared to other Type IIb supernovae.

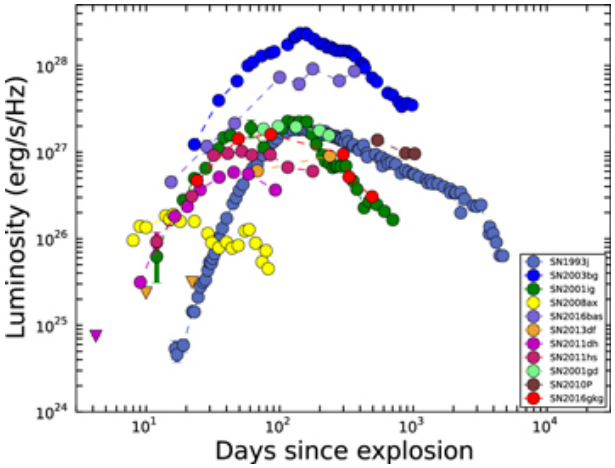

Figure 5.1: 5 GHz radio light curves of well-observed SNe IIb (Nayana et al. 2022).

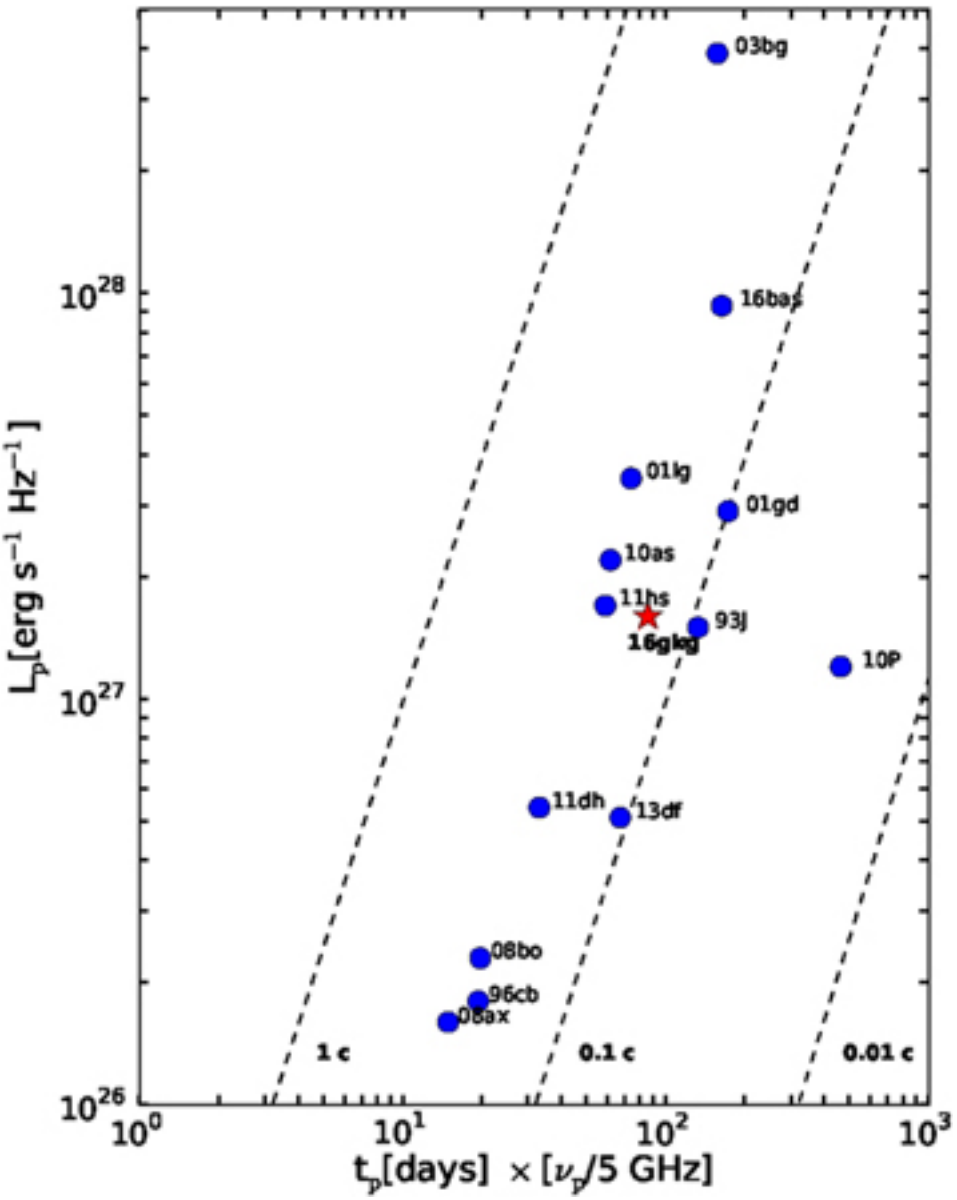

Figure 5.2: The peak radio spectral luminosities vs. time of the peak of the light curves are plotted for all well-observed SNe IIb in the literature (Nayana et al. 2022).

5.5 Nature of Progenitor from Radio Studies

There are only five SNe IIb that have progenitors identified from pre-explosion images. The stellar evolution model predicts that Type IIb supernovae which are core-collapse supernovae are presumed to occur when the star is a red supergiant. It is important to tie up the radio properties of these SNe with the inferences from pre-explosion imaging analysis. The progenitor of SN 1993J is identified to be a yellow supergiant star of radius $\sim$ 600 $R_{\odot}$ from pre-explosion images (Aldering et al. 1994). Similarly, an extended progenitor of radius $\sim$ 545 $\pm$ 65 $R_{\odot}$ was identified as the progenitor of SN 2013df (Schuyler D Van Dyk et al. 2014). SN 2008ax and SN 201dh are the other two SNe IIb with possible progenitor identifications in pre-explosion imaging (Folatelli et al. 2015). The progenitor of SN 2008ax was identified to be of radius $\sim$ 30-50 $R_{\odot}$. These estimates of progenitor radius from pre-SN image analysis are roughly consistent with the radio-derived properties - SN 2008ax has relatively compact progenitors with a higher shock velocity.

More massive progenitors experience stronger adiabatic cooling after the shock breakout because the beginning and strength of the cooling dip increase with progenitor mass. This suggests that fewer large progenitors may be to blame for many SNe IIb's absence of observed cooling dip. A young Wolf-Rayet (WR) star that had preserved a thin, low-mass shell of its original H envelope and exploded is consistent with the history of SN 2008ax as it has been observed. With the exception of a somewhat lesser H mass, SN 2008ax's general characteristics are similar to those of SN 1993J Soderberg et al. 2006. This could explain the observations that SN 2008ax's progenitor was a WR star rather than a K supergiant as was the case with SN 1993J, that SN 2008ax's light curve lacks a significant early-time peak, and that Hα is observed at faster velocities in SN 2008ax than in SN 1993J.

5.6 Summary

We present radio observations and modeling of a type IIb supernova, SN 2008ax. The radio observations span a frequency range of 4.86 GHz to 2.46 GHz at time $t \sim 4$ to 82 days post the supernova explosion. We model the radio flux measurements adopting the standard model of radio emission that arises due to the shock interaction of supernova ejecta with the CSM (Chevalier 1998, Chevalier 1989)initially suppressed by synchrotron self-absorption. We keep the normalization constants and the spectral and temporal evolution of optical depth and flux density as free parameters and execute a curve-fit algorithm using the Python curve-fit package. We obtain a reduced chi-square value of $\sim$ 3.206 for our best-fit model. While the model represents the data's overall spectral and temporal evolution, there are flux density enhancements above the model predictions at $t \sim 30$ days. We interpret this to be due to density fluctuations in the CSM possibly due to a variable mass-loss event in the progenitor's life close to the explosion. We estimate the shock radius, velocity, and post-shock magnetic

fields at multiple epochs post-explosion from the best-fit synchrotron light curves. The shock radii increase from $3.82 \pm 0.6 \times 10^{15}$ to $0.91 \pm 0.13 \times 10^{15}$ cm during $t \sim$ 14.414 to 3.5 days with a roughly constant shock velocity of v $\sim$ c. We compare the shock properties and radio luminosities of a sample of radio bright type IIb supernovae and find that the radio properties of SN 2008ax are indicative of a relatively compact progenitor star.

Bibliography

Aldering, Greg, Roberta M Humphreys, and Michael Richmond (1994). "SN 1993J: The optical properties of its progenitor". In: *The Astronomical Journal* 107, pp. 662–672.

Alsabti, Athem W and Paul Murdin (2017). *Handbook of supernovae*.

Bietenholz, Michael F, N Bartel, Megan Argo, et al. (2021). "The Radio Luminosity-risetime Function of Core-collapse Supernovae". In: *The Astrophysical Journal* 908.1, p. 75.

Chevalier, Roger A (1989). "Neutron star accretion in a supernova". In: *Astrophysical Journal, Part 1 (ISSN 0004-637X), vol. 346, Nov. 15, 1989, p. 847-859.* 346, pp. 847–859.

— (1998). "Synchrotron self-absorption in radio supernovae". In: *The Astrophysical Journal* 499.2, p. 810.

Crockett, RM, JJ Eldridge, SJ Smartt, et al. (2008). "The type IIb SN 2008ax: the nature of the progenitor". In: *Monthly Notices of the Royal Astronomical Society: Letters* 391.1, pp. L5–L9.

Dyk, Schuyler D van, Kurt W Weiler, Richard A Sramek, et al. (1994). "SN 1993J: The early radio emission and evidence for a changing presupernova mass-loss rate". In: *The Astrophysical Journal* 432, pp. L115–L118.

Folatelli, Gastón, Melina C Bersten, Hanindyo Kuncarayakti, et al. (2015). "The progenitor of the Type IIb SN 2008ax revisited". In: *The Astrophysical Journal* 811.2, p. 147.

Mostardi, R, W Li, and AV Filippenko (2008). "Possible Supernova in NGC 4490". In: *Central Bureau Electronic Telegrams* 1280, p. 1.

Nayana, AJ, Poonam Chandra, Anoop Krishna, et al. (2022). "Radio evolution of a Type IIb supernova SN 2016gkg". In: *The Astrophysical Journal* 934.2, p. 186.

Pastorello, Andrea, MM Kasliwal, RM Crockett, et al. (2008). "The Type IIb SN 2008ax: spectral and light curve evolution". In: *Monthly Notices of the Royal Astronomical Society* 389.2, pp. 955–966.

Roming, PWA, TA Pritchard, PJ Brown, et al. (2009). "Multi-wavelength properties of the type iib sn 2008ax". In: *The Astrophysical Journal* 704.2, p. L118.

Ryder, Stuart D, Elaine M Sadler, Ravi Subrahmanyan, et al. (2004). "Modulations in the radio light curve of the Type IIb supernova 2001ig: evidence for a Wolf–Rayet binary progenitor?" In: *Monthly Notices of the Royal Astronomical Society* 349.3, pp. 1093–1100.

Soderberg, AM, RA Chevalier, SR Kulkarni, et al. (2006). "The radio and X-Ray luminous SN 2003bg and the circumstellar density variations around radio supernovae". In: *The Astrophysical Journal* 651.2, p. 1005.

Taubenberger, S, H Navasardyan, JI Maurer, et al. (2011). “The He-rich stripped-envelope core-collapse supernova 2008ax”. In: *Monthly Notices of the Royal Astronomical Society* 413.3, pp. 2140–2156.

Van Dyk, Schuyler D, WeiKang Zheng, Ori D Fox, et al. (2014). “The Type IIb supernova 2013df and its cool supergiant progenitor”. In: *The Astronomical Journal* 147.2, p. 37.

Weiler, Kurt W, Nino Panagia, Marcos J Montes, et al. (2002). “Radio emission from supernovae and gamma-ray bursters”. In: *Annual Review of Astronomy and Astrophysics* 40.1, pp. 387–438.

18% Overall Similarity

Top sources found in the following databases:

- 15% Internet database
- Crossref database
- 3% Submitted Works database
- 13% Publications database
- Crossref Posted Content database

TOP SOURCES

The sources with the highest number of matches within the submission. Overlapping sources will not be displayed.

1	link.springer.com Internet	4%
2	astronomy.swinburne.edu.au Internet	2%
3	arxiv.org Internet	2%
4	annualreviews.org Internet	1%
5	"Handbook of Supernovae", Springer Science and Business Media LLC,... Crossref	1%
6	arxiv-vanity.com Internet	1%
7	en.wikipedia.org Internet	<1%
8	Roger A. Chevalier. "Synchrotron Self-Absorption in Radio Supernovae"... Crossref	<1%

9	prints.iiap.res.in Internet	<1%
10	academic.oup.com Internet	<1%
11	Roger A. Chevalier. "Synchrotron Self-Absorption in Radio Supernovae"... Crossref	<1%
12	handwiki.org Internet	<1%
13	wikimili.com Internet	<1%
14	coursehero.com Internet	<1%
15	authors.library.caltech.edu Internet	<1%
16	University of New York in Prague on 2016-03-15 Submitted works	<1%
17	nikki.jodymaroni.com Internet	<1%
18	researchgate.net Internet	<1%
19	"Supernovae", Springer Nature, 1990 Crossref	<1%
20	ned.ipac.caltech.edu Internet	<1%

21	Wesstwood College - CHL on 2010-06-29 Submitted works	<1%
22	aanda.org Internet	<1%
23	Lewis Ball, J.G. Kirk. "Radio Supernova 1987 A", Publications of the Ast... Crossref	<1%
24	Santa Barbara City College on 2014-03-14 Submitted works	<1%
25	everything.explained.today Internet	<1%
26	Bilkent University on 2023-06-13 Submitted works	<1%
27	Roger A. Chevalier, Claes Fransson. "Thermal and Non-thermal Emissi... Internet	<1%
28	Neutron Stars Theory and Observation, 1991. Crossref	<1%
29	University of Warwick on 2014-04-24 Submitted works	<1%
30	California Lutheran University on 2023-05-13 Submitted works	<1%
31	Xavier High School on 2016-08-24 Submitted works	<1%

Excluded from Similarity Report

- Bibliographic material
- Cited material
- Manually excluded text blocks
- Quoted material
- Small Matches (Less then 15 words)

EXCLUDED TEXT BLOCKS

A project report submitted in partial fulfillment for the award of the degree ofMast...

physics.iitm.ac.in

the partial fulfillment for theaward of

drttit.gvet.edu.in

has not been submitted for the award of any

Indian Institute of Science, Bangalore on 2020-06-01

project report has been approved as it satisfies the academic

Indian Institute of Science, Bangalore on 2020-06-01

ACKNOWLEDGEMENTSI would like to express my deepest appreciation and gratitu...

University of Birmingham on 2023-05-04

guidance, expertise, and

CSU, San Jose State University on 2023-05-20

friends and family for their unwavering support

CSU, San Jose State University on 2023-05-20

helped a lot in the completion of

fr.slideshare.net

Lastly, I am grateful to all the authors, researchers, and scholars whose works hav...

University of Bedfordshire on 2023-05-19

2.1Radio Emission 2.1.1

University of Durham on 2012-04-25

2 Synchrotron self absorption

Roger A. Chevalier. "Synchrotron Self-Absorption in Radio Supernovae", The Astrophysical Journal, 1998

Mass-loss rateIf

Poonam Chandra. "ELEVEN YEARS OF RADIO MONITORING OF THE TYPE IIn SUPERNOVA SN 1995N", The ...

Light CurveSN 2008ax is one of the best-monitored core-collapse SNe, starting wit...

arxiv.org

SN2008ax2008312

cfn-live-content-bucket-iop-org.s3.amazonaws.com

SN2008ax2008317

cfn-live-content-bucket-iop-org.s3.amazonaws.com

SN2008ax200841

cfn-live-content-bucket-iop-org.s3.amazonaws.com

200847

cfn-live-content-bucket-iop-org.s3.amazonaws.com

200858

cfn-live-content-bucket-iop-org.s3.amazonaws.com

SN2008ax2008516

cfn-live-content-bucket-iop-org.s3.amazonaws.com

The spectral index of a source is a measure of the dependence of radiative flux de...

wikimili.com